Theoretical Studies of Raman Scattering

Abdelsalam Mohammed

Department of Theoretical Chemistry
School of Biotechnology
Royal Institute of Technology
Stockholm, 2011

ISBN 978-91-7415-844-1
Printed by Universitetsservice US-AB, 2011
Stockholm, Sweden.

Abstract

Different theoretical approaches have been presented in this thesis to study the Raman scattering effect. The first one is response theory applied up to third order of polarization, where the determination of α, β and γ is used to calculate linear Raman scattering (resonance Raman scattering (RRS) and normal Raman scattering (NRS)), hyper Raman scattering (HRS) and coherent anti-Stokes Raman scattering (CARS), respectively. The response theory refers to adiabatic time-dependent density functional theory in the complex domain with applications on RRS and NRS, and to a recently developed methodology (Thorvaldsen *et al.* [105, 106]) for the analytic calculation of frequency-dependent polarizability gradients of arbitrary order, here with applications on CARS and HRS. Various systems have been studied with the response theory, such as explosive substances (DNT, TNT, RDX and H_2O_2), optical power limiting materials (platinum(II) acetylide molecules), DNA bases (methylguanine-methylcytosine) and other systems (Trans-1,3,5-hexatriene and Pyridine). We have explored the dependency of the calculated spectra on parametrization in terms of exchange-correlation functionals and basis sets, and on geometrical optimization.

The second approach refers to time-dependent wave packet methodology for RRS and its time-independent counterpart in the Kramers-Heisenberg equation for the scattering cross section, which reduces the calculation of the RRS amplitude to computation of matrix elements of transition dipole moments between vibrational wave functions. The time-dependent theory has been used to examine RRS as a dynamical process where particular attention is paid to the notion of fast scattering in which the choice of photon frequency controls the scattering time and the nuclear dynamics. It is shown that a detuning from resonance causes a depletion of the RRS spectrum from overtones and combination bands, a situation which is verified in experimental spectra.

The cross section of NRS has been predicted for the studied molecules to be in the order of 10^{-30} cm^2/sr. A further increase in sensitivity with a signal enhancement up to 10^4 to 10^5 is predicted for the RRS technique, while CARS conditions imply an overall increase of the intensity by several orders of magnitude over NRS. In contrast to RRS and CARS, the HRS intensity is predicted to be considerably weaker than NRS, by about four orders of magnitude. However, silent modes in NRS can be detected by HRS which in turn can provide essential spectroscopic information and become complementary to NRS scattering.

With the above mention methodological development for NRS, RRS, CARS

and HRS, we have at our disposal a powerful set of modelling tools for the four different Raman techniques. They have complementary merits and limitations which facilitate the use of these spectroscopes in applications of Raman scattering for practical applications, for instance stand-off detection of foreign substances.

Outlook

The remarkable evolution of large scale computations has in recent years created new ways of performing research. Simulations have, together with theoretical analysis and traditional experimental research, become an independent and useful tool to gain new knowledge. Ever since it became possible to carry out accurate calculations and computer simulations it has been a possible future scenario to design a material with specific properties and functions starting from basic, even, atomistic models. Modelling has in the past been very much descriptive and most often used to confirm results from experiments. Thanks to the fast increasing computing power and development of new modelling tools one can start to perform predictive modelling with the purpose to assist in the process to make new substances and drastically shorten the development times. The performance of materials can now be determined through modelling design which can unravel the crucial structure-function relationships. With the present thesis we show that modern modelling technology can be used to predict important and useful properties of molecules and molecular materials, namely their Raman cross sections and fingerprinting spectra. This knowledge can certainly be used to design experiments for special purposes. It is clear that the presumed theoretical efforts are actualized and motivated by the ever ongoing spectroscopic improvements, in particular by the development of tunable pulsed lasers at reduced costs, but also of detection techniques such as new types of CCD cameras.

A variety of methods in this thesis have been developed and applied to the molecular Raman problem and the applications cover by now a representative cross section of chemically and physically interesting molecules and effects. Theory has been found indispensable for interpreting and assigning the spectra. From the outset of the present state of the art we predict further development of theory and calculations of the Raman effect along several lines of research. One such line of development rests on electronic structure theory, taking account of the ever on-going advancements in that area. These advancements will be directly transferable to and assimilated in the spectroscopic techniques outlined in the present thesis, and will thus be of immediate use. In another line of development we see prolongation in terms of scales in length and time where ongoing work of so-called quantum mechanics - molecular mechanics technology paves the wave for simulations of Raman spectra of liquid and condensed phases, and where effects of dynamics, temperature and pressure adequately can be taken into account. One can predict further development of these theories more in conjunction with, or as direct generalizations of, the bound state electronic structure methods and computer codes, rather than by a development on their own. Applications will include further studies of environmental effects, fluorescence, pulse propagation and spectral purification using techniques presented in the thesis. Libraries of Raman spectra can be compiled and quickly screened for Raman detection in the field. The future is certainly wideopen and rich in prospects and will witness and ever-ongoing improvement

of the techniques. The simulation will never fully replace the experiment but it will serve as a substantial aid to make the experiment more effective and useful and its results more understandable.

Papers included in the thesis

Paper I.

Resonance enhanced Raman scattering from the complex electric-dipole polarizability: A theoretical study on N_2,
A. Mohammed, H. Ågren and P. Norman
Chem. Phys. Letter, **468**, (2009), 119-123.

Paper II.

Time-dependent density functional theory for resonant properties: resonance enhanced Raman scattering from the complex electric-dipole polarizability,
A. Mohammed, H. Ågren and P. Norman
Phys. Chem. Chem. Phys., (2009), **11**, 4549

Paper III.

Classification of Raman active modes of platinum(II) acetylides. A combined experimental and theoretical study,
A. Mohammed, B. Minaev, H. Ågren, M. Lindgren and P. Norman
Chem. Phys. Letter, **481**, (2009), 209-213.

Paper IV.

Ab initio *study of coherent anti-Stokes Raman scattering (CARS) of the 1,3,5-trinitro-1,3,5-triazacyclohexane (RDX) explosive*,
A. Mohammed, H. Ågren, A. J. Thorvaldsen and K. Ruud
Chem. Phys. Letter, **485**, (2010), 320-325.

Paper V.

Fluorescence and FTIR Spectra Analysis of Trans-A_2B_2-Substituted Di- and Tetra-Phenyl Porphyrins,
P. Sen, C. Hirel, C. Andraud, C. Aronica, Y. Bretonniere, **A. Mohammed**, H. Ågren, B. Minaev, V. Minaeva, G. Baryshnikov, H. Lee, J. Duboisset and M. Lindgren.
Materials, **8**, (2010), 4446-4475.

Paper VI.

Hyper Raman spectra calculated in a time-dependent Hartree-Fock method
A. Mohammaed, M. Ringholm, A. J. Thorvaldsen, K. Ruud and H. Ågren
Manuscript.

Paper VII.

Raman scattering at resonant or near-resonant conditions: A generalized short-time approximation
A. Mohammaed, Y.-P. Sun, Q. Miao, H. Ågren and F. Gel'mukhanov.
Manuscript.

Papers not included in the thesis

Self-assembly of propanethiol compounds on an Au(111) surface: Theoretical Investigation
M. Linares, U. Ekström, **A. Mohammed**, S. Stafström and P. Norman.
Manuscript.

My contribution to the included papers in this thesis

- I was responsible for all theoretical calculations and preparing the manuscripts for papers **I** to **IV**, including **VI**.
- In Paper **V** I performed all theoretical calculations and contributed to the discussion.
- I have been responsible for THT and DNA calculations and involved in preparing the manuscript for paper **VII**.

Acknowledgments

There are several people who contributed to this thesis in various ways, either by fruitful collaboration or constructive criticism and discussions. However, two of those people have left their finger-prints on this thesis, and therefore they deserve to have their contributions mentioned in more detail. Thus, it is fair not to treat them like any other, but to acknowledge them differently as it should be. These two people are prof. Hans Ågren and Prof. Patrick Norman.

I met Patrick Norman for the first time eight years ago, when I participated in the Modern Physics course during my undergraduate studies at Linköping University. He was the lecturer of this course and also two other courses later on, namely Quantum Mechanics, and Quantum Chemistry. I did enjoy listening to that young teacher, who presented the topics in a professional way. I also enjoyed the discussion with him outside the class, concerning some aspects which were related and unrelated to the courses. I was very curios about his research and admired his skills in particular problem solving. Three years later after we met I started my diploma work in his research group at the Division of Computational Physics. He was very supportive and putting time and effort to teach me the fundamentals of Quantum Chemistry and the small details of computing. I am very grateful to this man and owe him a lot for guidance and support for this and previous work.

Above all this, it was Patrick who introduced me to prof. Hans Ågren, who became my supervisor as a PhD student (Hans was also the supervisor of Patrick 15 years ago). Hans proved to be a pragmatic gentleman who has got unlimited ideas when it comes to put science into practice. It has been a great pleasure and honour to work with such a well known scientist, not just because he gave me enough time to think and do things freely, but also for his guidance along with very interesting projects where theory bridges with experiment. His encouragement was without boundaries and very helpful, particularly his supportive comments about my results. His great spirit and sense of humour didn't allow me to feel stressed during my three and half years of research with him. Hans, I am deeply thankful for your help and appreciate your kindness more than words can say.

Through Hans I got in contact with industry, i.e. Portendo AB and Swedish defence research agency (FOI). I would like to acknowledge the financial support from Portendo AB and the Energetic Materials group at FOI; most notably: Dr. Henric Östmark, Dr. Sara Wallin, Miss. Ida Johansson and Dr. Anna Pettersson for providing me with experimental data and showing me their lab.

With the initiative of Hans, to work with CARS project, I got in touch with Prof. Kenneth Ruud at Tromsø university. I spent almost one month in Tromsø to work with Kenneth's group. I would like to thank him for his help and hospitality during my stay, and I would like also to thank the members of his group, Dr. Andreas Thorvaldsen, Dr. Bin Gao and Mr. Magnus Ringholm for their support and fruitful collaboration in the CARS and hyper Raman projects.

My collaborators Prof. Mikael Lindgren, Prof. Boris Minaev, Prof. Faris Gel'mukhanov, Miss. Yuping Sun and Miss. Q. Miao deserve an acknowledgment for successful collaborations. To this list I would like to add Prof. Yi Luo for his great hospitality during my stay in China (the Nordic-China Symposium). The present and former members of our group at Theoretical Chemistry, I would like to thank all of them for providing a pleasant working atmosphere: Dr. Mathieu Linares, Dr. Marten Ahlquist, Dr. Arul Murugan, Dr. Zilvinas Rinkevicius, Dr. Ying Fu, Dr. Olav Vahtra, Dr. Kestutis Aidas, Prof. Kersti Hermansson, Mr. Guangjun Tian, Mr. Sathya Perumal, Mr. Xiao Cheng, Mr. Staffan Hellstrom, Mr. Weijie Hua and Mr. Fuming Ying.

Last, but certainly not least, many thanks to my family and relatives in Sweden and Iraq: Mr. Per Falk, Mrs. Gertrud Månsson Falk, Mr. Sverker Holmqvist, Mr. Robin Holmqvist, Mr. Kjell Holmqvist, the happy boy Einar Henriksson, Mrs. Erica Henriksson, Mrs. Hanna Månsson and many other good friends: Mr. Michael Stenrup and Mr. Hammed Al Najjar for their friendship and support throughout my work with this thesis.

Contents

1 Introduction **13**
- 1.1 A brief history of Optics . . . 13
- 1.2 Birth and development of Raman Spectroscopy . . . 14

2 Raman spectroscopy **19**
- 2.1 Raman scattering . . . 19
- 2.2 Linear Raman spectroscopy . . . 23
  - 2.2.1 Resonant and non-resonant Raman scattering . . . 23
  - 2.2.2 Raman cross sections . . . 23
  - 2.2.3 Instrumentation . . . 26
- 2.3 Nonlinear Raman spectroscopy . . . 28
  - 2.3.1 Coherent anti-Stokes Raman scattering (CARS) . . . 28
  - 2.3.2 Instrumentation . . . 28
- 2.4 Hyper Raman scattering (HRS) . . . 30

3 Theory **31**
- 3.1 Quantum mechanical theory . . . 31
  - 3.1.1 Born–Oppenheimer approximation . . . 32
  - 3.1.2 Pauli exclusion principle . . . 32
- 3.2 Self-consistent field theory . . . 33
  - 3.2.1 Hartree–Fock method (HF) . . . 33
  - 3.2.2 Kohn–Sham equation (KS) . . . 33
  - 3.2.3 Exchange and correlation functionals . . . 35
- 3.3 Vibronic theory . . . 36
  - 3.3.1 Time-dependent resonance Raman scattering . . . 36
  - 3.3.2 Linear coupling model (LCM) . . . 39
- 3.4 Response theory . . . 43
  - 3.4.1 Resonance Raman scattering (RRS) from the derivative of the polarizability tensor . . . 44
  - 3.4.2 Coherent anti-Stokes Raman scattering (CARS) . . . 46
  - 3.4.3 Hyper Raman scattering (HRS) . . . 47

4 Applications of linear and nonlinear Raman scattering 49
4.1 Linear Raman scattering 49
4.1.1 Stand-off detection of explosive substances 49
4.1.2 Applications of RRS to Biomolecules 53
4.2 Nonlinear Raman scattering 58
4.2.1 Coherent anti-Stokes Raman scattering (CARS) 58

Chapter 1

Introduction

1.1 A brief history of Optics

The word optics is derived from the Greek word optikos and refers to vision [41]. The laws of optics were though scientifically studied and discussed by philosophers throughout history already before the time of the Greek. It began with the development of lenses by the ancient civilization in Mesopotamia (land between the rivers, modern-day Iraq), where the earliest known lens namely the Nimrud lens [21] made of rock crystal was fabricated in Babylon. Theory of vision attracted many philosophers and the attention of scholars and might date back to ancient antiquity (800 B.C. to 500 A.D.). Curiosity and sought were the driving forces behind the study of this theory. Understanding the nature of such a phenomenon as vision was considered to be the key of locked secrets of the universe. During that time, two different theories [74] emerged about vision. The emission theory, supported by philosophers like Euclid and Ptolemy, proposed that sight worked by emitting rays of light from the eyes. In contrast, the intromission theory, which was advocated by Epicurus and his followers, stated that visual perception origins from particles emitted by an object and entering the eyes. Many centuries later, physical and physiological optics were significantly developed by scientists in the medieval Islamic world [56, 89]. One of these well known scientists was Alhasan Ibn al-Haytham who is called the father of optics, established and proved the vision theory through the use of experimentation [55, 89]. His book Kitab al-Manather (Book of Optics) which was translated into Latin in the 12th century, was dealing with the physical nature of light such as the color of sunset, shadows, rainbow, eclipses and many other physical phenomena [15].

The theory of modern optics was proposed and greatly developed by many famous scientists such as Newton, Huygens, Maxwell, Planck, Einstein, de Broglie, Compton, Bohr and many others. Their contributions have been considered to be revolutionary in the field of quantum mechanics in general and

quantum optics in particular. The latter deal with the application of the former to optical systems. For instance there are some phenomena in nature where light interacting with matter possesses not only wave–like (Huygens theory) but also particle–like feature (Newton theory), known as the duality of light. In fact the duality of light applies to all objects in nature including the macroscopic level, however, it is not possible to detect the wave properties for large systems due to the small wavelength which is beyond the experimental range of detection. In contrast, light–matter interaction at the microscopic scale can be studied and analysed by the use of spectroscopy. This technique has in fact already been provided by nature, e.g. the human eye which can detect the visible light and has the maximum sensitivity in the green region of the optical spectrum. The human eye does not, however, have the ability to detect light in the infrared which is far beyond our response region, or in the ultraviolet region, in contrast to many species like bees which can see ultraviolet light. The strong development in technology of spectroscopy in recent years has greatly advanced our understanding of the light matter duality and light behavior. Spectroscopy has also formed the bridge between experiment and theory in different fields of physics, chemistry and biology. It has become common practice today to identify substances, analyse structure and properties of functional molecules, by using Raman spectroscopy.

In this thesis we will shed light on the theory behind Raman spectroscopy in general and focus on various types of Raman techniques. To do so, we divide the work into two parts – linear and nonlinear Raman spectroscopy. The former is concerned with normal Raman and resonant Raman scattering, the latter is devoted to coherent anti-Stokes Raman scattering (CARS) and hyper Raman scattering (HRS).

1.2 Birth and development of Raman Spectroscopy

The Indian scientist Chandrasekhara Venkata Raman was fascinated by the deep blue color of the Mediterranean sea. However, he was unsatisfied with Lord Rayleigh's explanation that the color of the sea was just a reflection of the color of the sky, which was explained by the classical theory of light scattering for unchanged frequency in 1871. Thinking on the matter and working extensively on a series of measurements of light scattered by liquids as well as by some solids, Raman and his group in Calcutta managed in 1928 to show that the color of the sea was the result of the scattering of sunlight by the water molecules. However, the inelastic light scattering phenomenon had already been predicted a few years earlier by the Austrian physicist Adolf Smekal [58]. Smekal proposed that photons could be scattered inelastically by molecules and would consist of shorter and longer wavelengths in addition to the origin wavelength. Smekal also showed that the frequency shift between the incident and scattered light is due to the energy difference between two states of

the molecule. Meanwhile, two Russian physicists, Landsberg and Mandelstam observed light scattering with change of frequency by investigating Brillouin scattering from quartz. After all, the theoretical basis had been provided by Smekal, though his work was not widely known at that time. Moreover, the results of Landsberg and Mandelstam had been published after Raman's work was in print. For these reasons, Raman was considered to be the first who explained the phenomenon of the light scattering effect which was named after him and that earned him the Nobel prize in 1930.

The development of Raman spectroscopy, however, was relatively slow due to many reasons [37]. First, the Raman effect is very weak. Typically only one part in a thousand of the total intensity of the incident light is Rayleigh scattered, while for Raman scattering this value drops to one part in a million. Thus, as the Raman effect is quite weak, it is a major challenge to attenuate the light that is elastically scattered in order to detect the inelastically scattered Raman light. This might partly explain why the effect was not discovered earlier [37]. The second reason is that in all of the early light-scattering studies, the excitation source was sunlight and the samples used in the analysis were liquids. Furthermore, much of the early work in Calcutta was done by visual observation of color rather than precise measurements of the light wavelength, which Raman has described as being a plentiful task to do. However, these difficulties have been overcome and things changed dramatically after the discovery in 1960 of the laser. The birth of the laser technique thus stimulated the traditional field of molecular spectroscopy and Raman spectroscopy in various ways. It also allowed the molecular spectroscopest to record and analyse Raman spectra of a great variety of compounds, from deeply colored materials to highly fluorescent molecules. Besides, the laser technique has indeed provided a rapid development of fundamentally new methods, for instance in nonlinear spectroscopy. Soon after this major achievement of the laser discovery, Franken *et al.* [28] demonstrated nonlinear optical effects in different media produced by an intense electric field of a laser.

The new laser technology was also the master key for development of different kinds of Raman spectroscopes. We have today more than 25 types of linear and nonlinear Raman spectroscopy techniques [58]. The principal ones are widely used in areas such as chemical and material science, art restoration, and in military and biomedical applications. This holds for coherent anti-Stokes Raman scattering (CARS) and resonance Raman scattering (RRS) which are main topics in this thesis. The former is a nonlinear (four-wave mixing) technique based on the contributions of the nonlinear part of the induced dipole moment, and was first reported by Maker and Terhune in 1965 [19, 59]. However, the major important achievement and development for the application of this technique owes to Taran and coworkers in 1973 [90]. Resonance Raman is a linear two-photon scattering process, that first was experimentally observed by Shorygin in 1974 [14]. The use of resonance Raman spectroscopy has essential consequences for practical applications. Firstly, the absolute intensities are

much higher (3-6 orders of magnitude) than normal Raman scattering (NRS). The second important consequence is that the technique provides information about structural changes in excited states of molecules.

The quantum mechanical dispersion (QMD) theory of Raman scattering is based on Smekal's work. This theory includes an expression of the polarizability tensor ($\alpha_{\alpha\beta}$) derived from the time-dependent perturbation theory by Kramers, Heisenberg and Dirac (KHD) [49, 23]. However, this formalism contains a sum over vibronic states and is therefore complicated to use in practice. Albrecht and co-workers developed an approximation to the KHD expression and introduced two terms; the Franck–Condon (FC) and Herzberg–Teller (HT) terms which can be calculated if only few states are considered. They are in general difficult to calculate for larger molecules with many vibrational modes [54]. In contrast, there is a simple approximate expression from classical prolarizability theory which describes vibrational Raman scattering as an induced dipole moment that is linear in the applied field [53] (as outlined in Chapter 3 of this thesis). However, the classical prolarizability makes no mention of the role of the excited vibronic states. Placzek derived an expression to relate this theory to the QMD theory by indicating the role of the excited states and this expression was successfully applied in the non-resonance regime. Since these early contributions, different approximations have been used to calculate resonance Raman scattering. For instance, Peticolas and Rush [61, 92, 34] introduced transform theory based on the Kramers–Kronig transform of the absorption spectrum. Lee and Heller combined the KHD formula into a time-dependent formalism in terms of wave-packet dynamics [4, 35, 67, 85, 31, 94, 81, 69, 53, 58, 110]. With the introduction of 3rd generation synchrotron sources, resonant Raman scattering became measurable also in the X-ray region, unraveling many new physical effects. Major contributions to the theory of X-ray Raman scattering, both in time-independent or time-dependent formulations, were made by Gel'mukhanov and Ågren [31, 30].

Lee suggested that the Paczek-type polarizibility (PtP) tensor could be used in the resonance regime [53] when the lifetime of the intermediate electronic state is much shorter than the period of nuclear vibrations. In this case, the wave packet promoted in the intermediate state has no time to spread on the potential energy surface of this state. Consequently, one can neglect the sum over intermediate vibrational states when the lifetime is short [53]. A more rigorous short lifetime approximation, including the notion of a dephasing time of scattering due to an excitation detuned from resonance, is presented in paper VII of the present thesis. Other theoretical work on resonant Raman spectroscopy are based on wave packet propagation to describe nuclear motions on the ground and excited potential energy surfaces [4, 35, 67, 85, 31, 94, 81], few-states models based on the Kramers–Heisenberg formula [61, 92, 34], and on the complex polarization propagator approach (CPP) [77, 76, 45, 44]. The latter derivation was carried out in Paper I and II of the present thesis [63, 64]. The applications of resonant Raman spectroscopy described in this thesis focus

on the two latter strategies, that is complex polarization propagator approach and the Kramers-Heisenberg formula.

Chapter 2

Raman spectroscopy

This chapter is devoted to the description of the basic technology of linear and nonlinear Raman scattering. I consider four important spectroscopic phenomena which are relevant for this thesis. The first two arise from the linear interaction of a monochromatic radiation with a system, namely resonant Raman scattering (RRS) and non-resonant Raman scattering (NRS). The last two spectroscopic phenomena are coherent anti-Stokes Raman scattering (CARS) and hyper-Raman scattering (HRS) representing nonlinear effects. All four Raman scattering effects involve changes in the frequency of laser radiation as a result of its interaction with a system. Furthermore, each of these effects involves different techniques and principles and hence new applications and valuable information can result. I include also a brief overview of the experimental setup for these different techniques.

2.1 Raman scattering

The linear and nonlinear optical phenomena in Raman scattering describe the change of the molecular optical properties due to the presence of an electric field. Such interaction can be partly explained by classical theory of light scattering which in some respect can be regarded as a complementary view to a quantum mechanical treatment of light-matter interaction. From the quantum mechanical point of view, light and matter is dual in behavior, meaning that they display in some cases wave nature properties, like in diffraction, whereas at other instances, they show a behavior of particles [33]. Furthermore, these two complementary views of light as either a classical electromagnetic wave or a stream of photons can be used to describe the Raman effect, which is a result of inelastic interaction between light and matter. This interaction in turn can generate linear and nonlinear optical phenomena, depending on the strength of the applied electric field and the nature of the sample. For instance, the electric field intensities must be higher than typically 10^9 V/m to make the

contributions of the induced dipole moment large enough to create a nonlinear effect in the medium [47]. Such high electric field intensities can be reached with the use of giant-pulse lasers.

After this short introduction let us first consider linear scattering and in particular the situation when the frequency of incident light (stream of photons) ω_0 is far away from the molecular electronic absorption frequency ω_1 such that $\omega_\nu \ll \omega_0 \ll \omega_1$, where ω_ν is the vibrational frequency of the molecule (see Fig. 2.1). This is of course in line with the restriction of the photon wavelength (energy) which lies in between the visible and near-visible regions and corresponds to vibrational and electronic molecular excitation energies. In this case, the photon transfers its energy ($\hbar\omega_0$) to the whole molecule in order to displace the electron and produce an induced dipole moment. However, the electron remains bound because the large mass of the molecule does not allow such a transition. Consequently, most of the incident light (photons) is transmitted without change of frequency and this type of scattering is called Rayleigh scattering also known as elastic scattering (see Fig. 2.1).

The above mentioned case is the one most likely to occur for different conditions, in addition, there is also a possible situation where the photon can be considered as absorbed and the molecule makes a transition to a so-called virtual state which is indicated by a broken line in Fig. 2.1. This virtual state is not a stationary state neither it is a solution of time-independent Schrödinger equation and thus it does not correspond to a well-defined value of energy. However, this process of interaction or virtual absorption occurs under very short time of the time-scale τ, and hence the time-energy uncertainty relation still holds in this case, (see Fig. 2.1)

$$\tau\Delta E \geq \frac{1}{2}\hbar \tag{2.1}$$

where ΔE is the energy difference between the virtual and nearest resonant state (detuning energy). Now after this virtual absorption, the molecule will return back to its ground state through the process of de-excitation which gives rise to the scattered photon ω_s. Moreover, if the frequency of the scattered photon (ω_s) is analysed, there will in general be a characteristic frequency of the type ω_s=$\omega_0\pm\omega_\nu$. The new frequencies correspond to so-called Raman bands which collectively represent the normal Raman spectrum of the molecule. The Raman bands at frequencies less (greater) than the incident frequency ω_0 is referred to as Stokes (anti-Stokes) bands. The origin of the Stokes and anti-Stokes scattering may be explained in terms of energy transfer between the incident light (photons) and the scattering system. When the molecule is initially excited to a level above the ground state, the scattered photon will gain energy and is termed anti-Stokes scattering $\hbar(\omega_0+\omega_\nu)$. On the other hand if the molecule is initially at its lowest level (usually the ground state), the scattered photon will loose energy and is termed Stokes scattering $\hbar(\omega_0\text{-}\omega_\nu)$ (see Fig. 2.1).

When the detuning ΔE decreases, the photon energy is large enough (ω_1=ω_0+ ΔE) to excite the molecule into the electronic state S_1 which become absorbing. In this case the molecular properties such as the polarization becomes different and require more complex analysis than in the non-resonant case [77, 75, 63, 64]. It is also worthwhile to mention that when the electromagnetic force field acts on the molecule, the electron density as well as the nuclei are subjected to a force that might alter their motion. However, the nuclei are much heavier than electrons and they are highly likely to remain with unaltered motions. Furthermore, after a specific time the molecule will relax back to different vibrational states associated with a scattered photon of different frequencies, i.e. fundamental (0–0), (0–1), first overtone (0–2), second overtone (0–3), and so forth. These different de-excitations depend on the shift between the potentials of ground and excited states (see paper VII).

Our discussion so far has centered mostly on the linear Raman effect (resonance and non-resonance scattering) and described the incident light as a stream of photons that act on a molecule. We will now turn to a discussion about nonlinear Raman scattering, using classical electromagnetic waves to represent the incident light which interact with the system. When a system is illuminated with a monochromatic radiation E(t) of frequency ω which is sufficiently large (Q-switched laser), the scattered radiation can be found to have a frequency of $2\omega - \omega_\nu$ (see Fig. 2.1). This frequency arises from the first-order nonlinear induced dipole ($\mu^{(2)} = \frac{1}{2}\beta : EE$), where β is the first-order non-linear hyperpolarizability [39]. Such scattering is called Stokes hyper Raman scattering. Actually both hyper Rayleigh scattering and anti-Stokes hyper Raman scattering are involved in such nonlinear scattering, however, in this thesis we pay attention only to the Stokes type.

We consider now another type of nonlinear Raman scattering, namely coherent anti-Stokes Raman scattering (CARS). CARS originates in a third-order nonlinear optical process ($\mu^{(3)} = \frac{1}{6}\gamma : EEE$) which utilizes two relatively high-powered laser beams, where a pump and a Stokes laser beam, with angular frequencies ω_p and ω_s and with $\omega_p > \omega_s$, are focused into a sample. Due to the laser mixing, a new coherent beam is generated in the medium at the anti-Stokes frequency of ω_{cars}=$2\omega_p - \omega_s$ [107] in the forward direction, and collinear with the pump beams (ω_p). This new beam results from the inelastic scattering of the pump beams (ω_p) by the molecular vibrations, which in turn is coherently driven by the beams ω_p and ω_s. The CARS signal is significantly enhanced when $\omega_p - \omega_s$ coincides, or is tuned to be resonant with a molecular vibration ω_ν (see paper III).

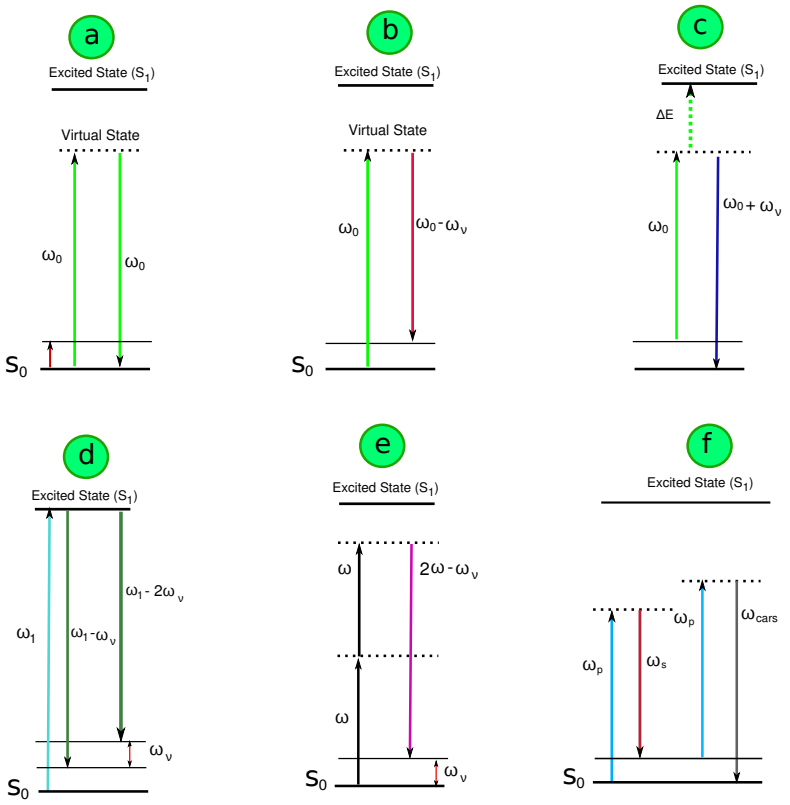

Figure 2.1: Different optical processes of scattering.(a) Rayleigh, (b) non-resonance Raman scattering (Stokes), (c) non-resonance Raman scattering (anti-Stokes), (d) resonance Raman scattering (RRS), (e) hyper-Raman scattering (HRS) and (f) coherent anti-Stokes Raman scattering (CARS).

2.2 Linear Raman spectroscopy

2.2.1 Resonant and non-resonant Raman scattering

Raman spectroscopy is a powerful and widely used technique to probe the structure and function of molecular materials and condensed matter. It relies on inelastic scattering of monochromatic light, usually from a laser in the visible, near infrared or near ultraviolet ranges. When the directed light passes through a sample, a fraction is scattered in all directions. The Raman effect can occur with a change in vibrational, rotational or electronic energy. As the signal is very sensitive to the chemical structure of a molecule, the Raman signal becomes a reporter of the specific structure and hence gives a fingerprint of the molecule. Raman spectroscopy can provide a further 10^3 to 10^6 increase in sensitivity by operating at the resonance frequency of the sample molecule. In resonance Raman scattering (RRS), the energy of the incoming laser is adjusted such that it coincides with an electronic transition of the molecule. The main disadvantage of RRS is the increased risk of fluorescence and photo-degradation of the sample due to the increased energy of the incoming laser light.

2.2.2 Raman cross sections

Consider a single molecule located at the origin 0 of a space-fixed Cartesian system X, Y, Z (Fig. 2.2). Assume that the incident radiation to be a monochromatic non-divergent parallel beam of small cross section (laser excitation), with angular frequency ω, and that the scattered radiation can be observed along a certain direction (non-divergent) beam by arranging the experimental conditions. We assume also that the wavelength of the incident radiation $\overline{E}$ is large compared to to the size of the molecule. For instance, the wavelength of light in the visible and ultraviolet regions of the electromagnetic spectrum is of the order of 100 nm, while a typical bond length in a molecule is of the order 1 Å=0.1 nm. Bearing in mind these idealized conditions we will consider a common macroscopic experimental setup to have a beam incident in the Z-direction and polarized along the Y-direction. The detection of the Raman scattering intensity is then made in the X-direction ($I_s \propto \overline{\langle \mu^{\mathrm{ind}} \rangle_{fi}^2}$). In this situation the induced polarization oscillating in the YZ-plane is detected as a response to the molecule-radiation interaction and the square amplitude of the polarization becomes [64, 63]

$$\overline{\langle \mu^{\mathrm{ind}} \rangle_{fi}^2} = \left[\alpha_{YY}^{fi}(\omega) E_Y^{\omega} e^{-i\omega t} + \text{c.c.}\right]^2 + \left[\alpha_{ZY}^{fi}(\omega) E_Y^{\omega} e^{-i\omega t} + \text{c.c.}\right]^2, \qquad (2.2)$$

where $\alpha^{fi}(\omega)$ is the polarizability of the molecule, E_Y^{ω} is the amplitude of the electric field and the subscript fi denotes a transition moment between the initial and final vibrational states and where the integration over electronic coordinates has been carried out so that μ^{ind} is a function of the nuclear coordinates. The overbar indicates that an orientation averaging is to be performed

in correspondence with a randomly oriented molecular configuration [63]. The Raman intensity relevant to the above mentioned experimental conditions goes as the ratio of radiation power $d\Phi$ in a conical beam of solid angle $d\Omega$ (Fig. 2.2). The detected radiation is due to the induced polarization in the sample; the expression for its intensity is given by [57, 58]

$$I_s = \frac{d\Phi}{d\Omega} = \frac{\omega_s^4 \overline{\langle \mu^{\mathrm{ind}} \rangle_{fi}^2}}{32\pi^2 \varepsilon_0 c^3} = I_0 \frac{d\sigma}{d\Omega}, \tag{2.3}$$

where c is the speed of light, ε is the vacuum permittivity and where it is assumed that I_s increases linearly with the incident intensity ($\mathrm{I_0}=\frac{1}{2}c_0\varepsilon_0 E_Y^2$) [13]. Furthermore, the cross sections σ and $\frac{d\sigma}{d\Omega}$ are often given instead of the scattered intensity I_s because they are independent of $\mathrm{I_0}$. The cross section σ can also be defined as an effective geometrical area of the molecule for removing light from the incident beam [13], and therefore it has the dimensions of an area. However, for practical reasons, it is preferable to make the measurement of the scattered light in a certain direction with a limited acceptance angle as we indicated before, thus, we differentiate the cross section with respect of the solid angle $\mathrm{d}\Omega$ to become as $d\sigma/d\Omega$. In this case the spatial distribution (probability distribution) of the scattered beam can be easily measured by counting the rate at which particles (photons) incident on detectors located at different positions around the target. It is also worthwhile to mention that the cross sections are in fact molecular properties that are dependent upon other experimental parameters. It is well known that Raman scattering is incoherent which means that that the intensity of an assembly of N molecules at normal temperature (in lowest vibrational state ν_k^i=0) is N times that from an individual molecule. However, not all molecules will be in the ν_k^i=0 state, some of them may populate the higher vibrational states (ν_k^i=1, 2, ...). Thus, we need to consider the Bolzmann distribution law in our expression of the cross section [64, 63].

Another common experimental situation in Raman scattering spectroscopy is to determine the scattered intensity by counting the number of photons N_s, with an angular frequency ω_s that are scattered in an element of solid angle $\mathrm{d}\Omega$ falling on the detector in a given period of time (unit time) according to

$$I_s = \frac{N_s \hbar \omega_s}{d\Omega} \tag{2.4}$$

Now if we keep $\mathrm{d}\Omega$ as a constant which is a usual experimental situation, then $\mathrm{N_s}$ becomes proportional to $\frac{I_s}{\hbar\omega_s}$ and has units of photon counts per second. To illustrate the latter approach, we will use the diatomic molecule $\mathrm{N_2}$ as an example to account the number of scattered photons with frequency ω_s in $\mathrm{d}\Omega$ per unit of time, when the molecule has been illuminated by the electric field. A typical experimental value of the transition polarizability $(\alpha)_{fi}$ measured on the Q branch in the Raman spectrum (vibration-rotation) of $\mathrm{N_2}$ is 5.0×10^{-42} C

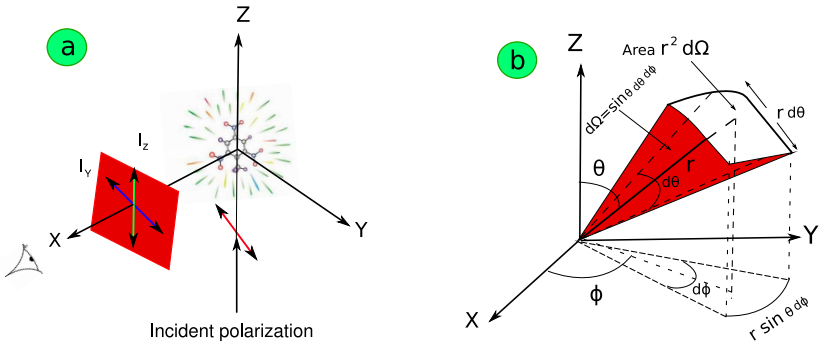

Figure 2.2: (a) Raman scattering from a single molecule: geometry for Z(YZ)X measurement. (b) An element of solid angle $d\Omega$ is defined from small section of a surface of sphere of radius r.

V^{-1} m^2. Further assume that the electric field amplitude is E_0=10^6 V m^{-1} with a wavelength of λ=488.0 nm (ν_0=2.0492 $\times$ 10^5 m^{-1}). This would correspond to an irradiance I_{ir}=10^{10} W m^{-2} (I_{ir}=$\frac{1}{2}c_0\epsilon_0 E_0$) which can be reached with a laser of power 1 W focused to a spot with an area of 10^{-10} m^2. We find that $(\mu^{\text{ind}})_{fi}$=5 $\times$ 10^{-36} C m (μ^{ind}=α.E_0) and ν_s=1.8160 $\times$ 10^6 m^{-1} (knowing that the N_2 vibration frequency is ν=2.332 $\times$ 10^5 m^{-1}). Using Eq (2.3) and calculating k=$\frac{c\pi^2}{2\varepsilon_0}$=1.671 $\times$ 10^{20} C^{-1} V m^2 s^{-1}. It gives I_s =4.4 $\times$ 10^{-26} W $sr^{-1}$$molecule^{-1}$, further the energy of the scattered photon is $\hbar\omega_s$=3.0 $\times$ 10^{-19} J. Putting dΩ=1, I_s =4.4 $\times$ 10^{-26} and $\hbar\omega_s$=3.0 $\times$ 10^{-19} in Eq (2.4) and accounting the number of scattered photons N_s, we find that one scattered photon per steradian per second would require about 10^7 molecules in the focal volume. For instance, a standard focal volume is $10^{-6}$$cm^3$ for a gas at standard temperature and pressure contains 3 $\times$ 10^{13} molecules. Moreover according to the above argument we can expect scattering of the order of 10^6 photons per steradian per second. For liquids the same focal volume contains about 6 $\times$ 10^{15} molecules which gives scattering of the order of 2 $\times$ 10^{19} photons per steradian per second.

2.2.3 Instrumentation

In modern Raman spectrometers (Fig. 2.3), lasers are used as photon sources due to their highly monochromatic nature and high beam flux. This is necessary as the Raman effect is weak, typically the Stokes lines are 1000 times weaker than the Rayleigh scattered component. In the visible spectral range, Raman spectrometers use filters to cut out the signal from a very narrow range centered on the frequency corresponding to the laser radiation. Further, most Raman spectrometers for material characterization use a microscope to focus the laser beam to a small spot (1-100mm diameter). Light from the sample passes back through the microscope optics into the spectrometer. The Raman shift radiation is detected with a charge-coupled device (CCD) detector, and a computer is used for data acquisition and curve fitting. These factors have helped Raman spectroscopy to become a very sensitive and accurate technique. Fig. 2.3 illustrates, in a block diagram as well as in symbolic fashion, the general arrangement of the components of Raman spectroscopy (the actual spectrometer design is shown in Fig. 2.3,b). The block diagram shows the necessary equipment that is needed for obtaining a Raman spectrum, i.e. a source of high-intensity monochromatic light, a sample which does not require any particular preparation (gas, liquid, or solid), a double monochromator (filter) to reject stray light and a charge-coupled device (CCD) detector commonly used nowadays for Raman spectroscopy.

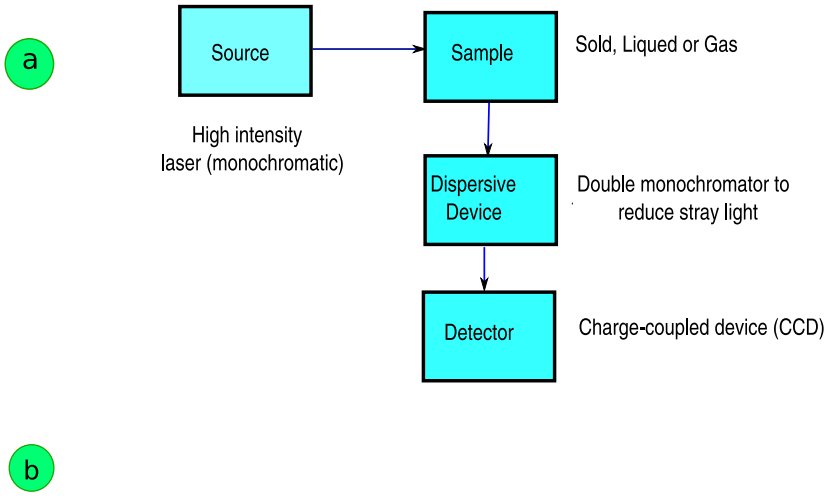

Figure 2.3: (a) Block diagram for Raman spectroscopy. (b) Raman experimental setup is taken from FOI (Swedish Defence Research Agency).

2.3 Nonlinear Raman spectroscopy

2.3.1 Coherent anti-Stokes Raman scattering (CARS)

The first observation of coherent anti-Stokes Raman scattering (CARS) was made by Maker and Terhune in 1965 [59]. Since this initial experiment, and the development of new lasers of high power and narrow line widths such as Nd-YAG and tunable dye lasers, the CARS experiment has become much more convenient and much progress has been made in its application. Further gain of the advances in laser sources has been utilized to improve CARS spectra of gases, liquids and solids. Thus, CARS has become a powerful tool in diagnostic applications in different environments where resolution and signal levels are limiting factors. CARS is a coherent technique which means that the signal is contained in a coherent laser beam. Furthermore, the origin of this signal lies in the response of the molecule to the applied electric field. The product of electric field amplitudes gives rise to an induced second-order nonlinear optical polarization in the molecule. In this optical process two laser beams of frequencies ω_p (pump) and ω_s tunable (Stokes) are used, where $\omega_p > \omega_s$. These two beams are focused together in a sample and converted to a laser like beam due to third order nonlinear optical mixing (see Fig. 2.4) [65, 107]. Moreover, the emitted laser beam is generated in the medium at frequency $\omega_{\text{cars}} = 2\omega_p$-$\omega_s$ in the anti-Stokes region and is many orders higher in intensity than spontaneous Raman scattering. The principle behind CARS is that the beam at the frequency ω_{cars} is resonantly enhanced when ω_p- ω_s is tuned to a Raman band. This technique has thus the advantage of obtaining a much stronger Raman signal, and has also the advantage that the back scattered anti-Stokes Raman signal is coherent with the reference beam, which allows the use of interferometric optical imaging techniques.

2.3.2 Instrumentation

Fig. 2.4 (a) shows a schematic experimental set up of CARS. It consists of a Nd:YAG-laser with frequency doubling and a Dye-laser. The latter is a tunable (Stokes) laser in the visible and is needed since it is very difficult to build a pulsed laser stable in frequency and intensity. The Nd:YAG-laser beam splits into two beams by a splitter, one pump beam with fixed frequency (ω_p) and a probe beam created by the Dye-laser with frequency (ω_s). There are also three more splitters and one lens to focus and cross the beams collectively into the sample to create a four wave mixing process. The result is a coherent beam at the anti-Stokes frequency (ω_{cars}) which is well separated from all incoming beams. The beam is then focused onto the entrance slit of a spectrometer/monochromator and detected with a CCD camera.

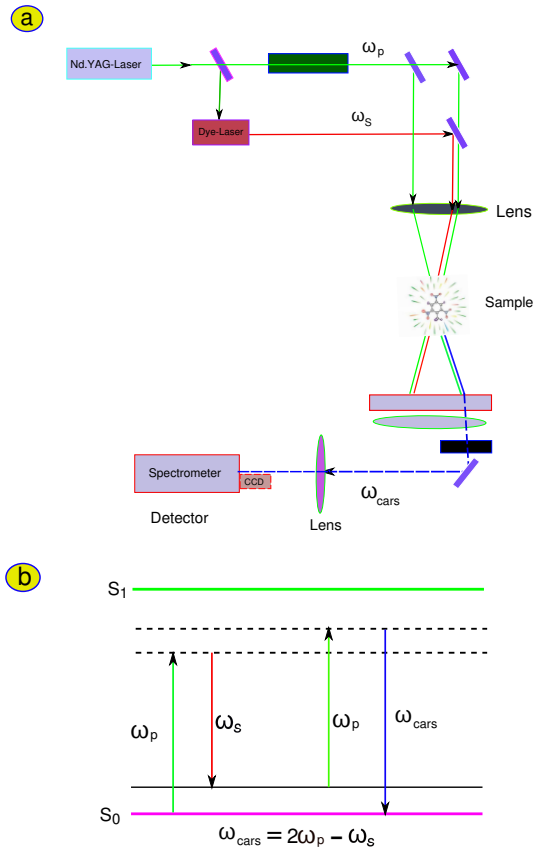

Figure 2.4: (a) Schematic instrumental setup of CARS, (b) CARS energy level diagram showing the scattering process: ω_p and ω_s is the pump laser beam and the Stokes laser frequency, respectively.

2.4 Hyper Raman scattering (HRS)

Hyper Raman scattering (HRS) was first predicted by Decius and Rauch [22] in 1959 and six years later the first experimental observation was made and reported by Terhune *et al.* [104]. HRS is a non-linear three-photon process which is associated with the first-order hyperpolarizability tensor β (see section 3.4). The interaction of two photons with frequencies ω_1 and ω_2 (usually ω_1=ω_2) with a sample causes an annihilation of these two incident photons and a creation of one scattered photon with frequency ω_s =$2\omega_1 \pm \omega_{vib}$, where ω_{vib} is the ground-state vibrational frequency of the sample, $2\omega_1 - \omega_{vib}$ ($2\omega_1 + \omega_{vib}$), is Stokes hyper Raman scattering (anti-Stokes hyper Raman scattering). The characteristic polarization of the scattered radiation is different from those of the incident radiation and the intensity as well as the polarization depend on the direction of observation. Furthermore, the intensity of HRS is [112, 87, 71]

$$I_{HR} \propto \sum_{\alpha\beta} \langle |\beta'_{\alpha\beta\beta}(\omega_s, Q)|^2 \rangle, \quad I_R \propto \sum_{\alpha\beta} \langle |\alpha'_{\alpha\beta}(\omega_s, Q)|^2 \rangle, \tag{2.5}$$

where $\beta'_{\alpha\beta\beta}$ is the α, β element of the hyperpolarizability derivative ($\frac{\partial\beta}{\partial Q}$), with respect to the normal coordinate Q and I_R is the intensity of non-resonant Raman scattering. Although HRS is a weak process estimated to be four to five orders of magnitude weaker than NRS [3], it has a complementary advantage due to its different symmetry selection rules. For instance, the ω_{vib} frequencies which are observed in HRS can be different from those observed in normal Raman scattering (NRS) and infrared absorption (IR). Hence, the modes, silent both in NRS and IR spectra, can be detected by HRS which in turn can provide essential spectroscopic information and become complementary to linear Raman scattering and infrared absorption [47, 91]. Therefore, the interest in the HRS technique lies in its potential as source of valuable spectroscopic information.

Chapter 3

Theory

3.1 Quantum mechanical theory

At the beginning of the twentieth century, electrons were found experimentally to give diffraction patterns when they passed through a double slit in a similar way as light waves. This experimental evidence has suggested that atomic particles were also wave–like in nature and it was therefore reasonable to assume that a wave equation could represent the behavior of atomic particles. In 1926 the Austrian physicist Erwin Schrödinger, managed to derive a wave equation which describes the motion of electrons and which came to have the same central importance to quantum mechanics as Newton's laws of motion have in classical mechanics. The Schrödinger equation describes the form of the probability waves that govern the motion of small particles, and it specifies how these waves are altered by external influence. Schrödinger had also established the correctness of the equation by applying it to the hydrogen atom, predicting many of its properties with remarkable accuracy. Furthermore, this equation is used extensively in atomic, nuclear, and solid-state physics. Nowadays, advanced computational techniques make heavy use of super-computers to solve the Schrödinger equation for different model systems in order to determine the electronic structure of atoms and molecules. The equation for general systems (n electrons and N nuclei) reads as

$$\hat{H}\left|\Psi\right\rangle = E\left|\Psi\right\rangle. \tag{3.1}$$

where $\hat{H}$ is the total non-relativistic Hamiltonian operator, Ψ is the eigenfunction and E is the energy of the system. Writing out all the terms in atomic units, the Hamiltonian is expressed as

$$\hat{H} = -\sum_{i=1}^{n}\frac{1}{2}\nabla_i^2 - \sum_{a=1}^{N}\frac{1}{2N_a}\nabla_a^2 - \sum_{i=1}^{n}\sum_{a=1}^{N}\frac{Z_a}{r_{ia}} + \sum_{i=1}^{n}\sum_{j>i}^{n}\frac{1}{r_{ij}} + \sum_{a=1}^{N}\sum_{b>a}^{N}\frac{Z_a Z_b}{R_{ab}}. \tag{3.2}$$

The first two terms in Eq 3.2 correspond to the kinetic energy of the n electrons and the N nuclei, respectively, and N_a is the ratio of the mass of nucleus a to the mass of an electron; the third term represents the Coulomb attraction between electrons and nuclei; the fourth and fifth terms represent the repulsion between electrons and between nuclei, respectively. Since Eq 3.1 can be solved analytically only for a single particle, one needs to make an approximation to solve this equation for large systems.

3.1.1 Born–Oppenheimer approximation

The solution of the Schrödinger equation for one particle can be achieved in a straightforward way, while for larger systems this is a formidable task to face. In many particle systems the separation of the total wave function into an electronic and a nuclear part is not possible without the *Born–Oppenheimer approximation*. In this approximation, we suppose that the nuclei, being much heavier than the electrons, move relatively slowly and can be considered as stationary while the electrons move around them. Therefore, instead of trying to solve the Schrödinger equation for all particles simultaneously, it is possible to regard the nuclei as fixed in position and to solve the Schrödinger equation for the electrons in the static electric potential arising from the nuclei [6]. It is then possible to separate the total wave function (by invoking this approximation) into a product of two parts referring to the electronic and nuclear wave functions.

The electronic Schrödinger equation reads

$$\hat{H}_{\text{elec}}\Phi_{\text{elec}} = E_{\text{elec}}\Phi_{\text{elec}}. \tag{3.3}$$

where the electronic wave function can be written as a function of electronic coordinates and parametrically of nuclear coordinates:

$$\Phi_{\text{elec}} = \Phi_{\text{elec}}(r_i; R_a). \tag{3.4}$$

For a fixed set of locations R_a of the nuclei. The electronic Hamiltonian is

$$\hat{H}_{\text{elec}} = -\sum_{i=1}^{n} \frac{1}{2}{\nabla_i}^2 - \sum_{i=1}^{n}\sum_{a=1}^{N} \frac{Z_a}{r_{ia}} + \sum_{i=1}^{n}\sum_{j>i}^{n} \frac{1}{r_{ij}}. \tag{3.5}$$

where n is the number of electrons in the field of N point charges. The first term in Eq 3.5 is the operator for the kinetic energy of the electrons, the second term represents the Coulomb attraction between electrons and nuclei and the last term represents the repulsion between electrons [102].

3.1.2 Pauli exclusion principle

For the interchange of any pair of electrons (half-integral spin), the total wave function must be antisymmetric and there is a restriction on the number of

electrons that can occupy the same state, in fact it is forbidden for two electrons to occupy the same state, something that is called the *Pauli exclusion principle*. Electronic wave functions that satisfy the Pauli principle are often written in terms of *Slater determinants*. The general form of a Slater determinant composed of the spin orbitals χ_1, χ_2, ..., χ_n and containing n electrons is

$$\psi(x_1, x_2, ..., x_n) = \frac{1}{\sqrt{N!}} \begin{vmatrix} \chi_i(x_1) & \chi_j(x_1) & . & . & . & \chi_n(x_1) \\ \chi_i(x_2) & \chi_j(x_2) & . & . & . & \chi_n(x_2) \\ . & . & . & . & . & . \\ . & . & . & . & . & . \\ . & . & . & . & . & . \\ \chi_i(x_n) & \chi_j(x_n) & . & . & . & \chi_n(x_n) \end{vmatrix}, \quad (3.6)$$

where the factor $(1/N!)^{1/2}$ is a normalization constant and x_n indicates both spatial and spin coordinates of the n:th electron. The electronic state is fully antisymmetric under the interchange of any pair of electrons, because this operation corresponds to the interchange of two rows in the determinant. Furthermore, if any two spin orbitals are the same, then the determinant vanishes because it has two columns in common.

3.2 Self-consistent field theory

3.2.1 Hartree–Fock method (HF)

The Hartree–Fock (HF) method is used to solve the electronic Schrödinger equation in an approximate way. It assumes that the wave function can be approximated by a single Slater determinant made up of one spin orbital per electron. It simply casts the exact many-electron wave function into a set of one electron wave functions. A solution of these non-linear equations can iteratively be solved by applying so-called self–consistent field theory. The main idea of this numerical method is to replace the electron–electron interaction by an average effective potential created by other electrons. It means that the multi-electrons problem reduces into a one electron problem which leads to relatively low computational cost and reasonable prediction of the exact energy. However, this is a rather crude approximation because in many systems the electron correlation effects (the difference between the HF energy and the exact energy on the basis set) can simply not be neglected and therefore we need to use a better approach to deal with such a problem.

3.2.2 Kohn–Sham equation (KS)

The basic idea of density functional theory for any systems of electrons is the one to one mapping between the external potential and the electron density: $v(\mathbf{r}) \leftrightarrow \rho(\mathbf{r})$ [42]. According to this theory, which was proved in 1964 by Hohenberg and Kohn [38], all properties are a functional of the electron density.

The density determines the potential from which we can get the Hamiltonian which in turn determines the energy and the total wave function Ψ. Knowing the total wave function is leading then to the determination of all physical properties. Hohenberg and Kohn also showed (second Hohenberg–Kohn theorem) that for a given potential $v(\mathbf{r})$, which corresponds to the ground state energy $E_0[\rho]$, the energy functional $E[\rho]$ has its minimum equal to $E_0[\rho]$ at the ground state density:

$$E_0 = \min_{\rho} E[\rho] = \min_{\rho} \left[\int d\mathbf{r} v(\mathbf{r})\rho(\mathbf{r}) + T[\rho] + V_{\mathrm{ee}}[\rho] \right] \tag{3.7}$$

where $\int d\mathbf{r} v(\mathbf{r})\rho(\mathbf{r})$ is the energy of the electrons in the external potential, $T[\rho]$ is the electronic kinetic energy functional and $V_{\mathrm{ee}}[\rho]$ is the electron-electron interaction energy functional. The explicit expression of the last two terms, $T[\rho]$ and $V_{\mathrm{ee}}[\rho]$, are unknown.

Kohn and Sham on the other hand presented a one-electron formalism to obtain the energy from the N-electron density. They considered a system of N non-interacting electrons, moving in a local potential $v_s(\mathbf{r})$, that leads exactly to the same density as the system of interacting electrons with potential $v(\mathbf{r})$. Provided such a system, the electron density is defined by the sum of the densities of the $N/2$ doubly occupied one electron orbitals,

$$\rho(\mathbf{r}) = 2 \sum_{i}^{occ} |\psi_i(\mathbf{r})|^2 \tag{3.8}$$

and the electronic energy functional is given by:

$$E[\rho] = T_s[\rho] + V_{\mathrm{ne}}[\rho] + J_{\mathrm{ee}}[\rho] + E_{\mathrm{xc}}[\rho] \tag{3.9}$$

where, $T_s[\rho]$ is the kinetic energy of non-interacting electrons, $V_{\mathrm{ne}}[\rho]$ represents the electron-nuclei interaction and the Hartree term, $J_{\mathrm{ee}}[\rho]$ is the Coulomb interaction among the electrons:

$$T_s(\rho) = -\frac{\hbar^2}{2m} \sum_{i=1}^{N} \int \mathrm{d}\mathbf{r} \psi_i^*(\mathbf{r}) \nabla^2 \psi_i(\mathbf{r}) \tag{3.10}$$

$$V_{\mathrm{ne}}[\rho] = \int \mathrm{d}\mathbf{r} v^{\mathrm{ext}}(\mathbf{r})\rho(\mathbf{r}) \tag{3.11}$$

$$J_{\mathrm{ee}}[\rho] = \frac{e^2}{2} \int \mathrm{d}\mathbf{r} \int \mathrm{d}\mathbf{r}' \rho(\mathbf{r})\rho(\mathbf{r}')/|\mathbf{r} - \mathbf{r}'| \tag{3.12}$$

The last term in Eq (3.9) is defined as the exchange correlation energy functional $E_{\mathrm{xc}}[\rho]$. It compensates the electron-electron interaction V_{ee} as being described only by the Coulomb interaction J_{ee} and for the kinetic energy functional which describes the kinetic energy for non-interacting electrons:

$$E_{\mathrm{xc}}[\rho] = V_{\mathrm{ee}} - J_{\mathrm{ee}}[\rho] + T[\rho] - T_s[\rho] \tag{3.13}$$

The electronic ground state density can be found by solving the Kohn–Sham equations given by [42]

$$\hat{H}^{\mathrm{KS}}\psi_i = \left[-\frac{\hbar^2}{2m}\nabla^2 + v^{\mathrm{ext}} + \frac{e^2}{2}\int \mathrm{d}\mathbf{r}\frac{\rho(\mathbf{r}')}{|\mathbf{r}-\mathbf{r}'|} + \frac{\delta E_{\mathrm{xc}}[\rho]}{\delta\rho(r)}\right]\psi_i = \epsilon_i\psi_i \quad (3.14)$$

3.2.3 Exchange and correlation functionals

As mentioned previously, an exact expression for $E_{\mathrm{xc}}[\rho]$ is not known and thus, several schemes have been developed to obtain a good approximation for those functionals. The first approximation was applied for a homogeneous electron gas or an electron gas with slow varying density as in metals. This approximation is known as the local density approximation (LDA) and it works surprisingly well despite its quite crude nature. However, the density changes rapidly in most molecules, and therefore does not follow the assumption to be slowly varying. This problem has been solved by considering density fluctuations via the gradient of the density. It in turn paved the way for the development of so-called generalized gradient approximations (GGAs). By now a large number of the GGA functionals for both correlation and exchange have been developed for different applications. One of the most popular and widely used functional is the so-called hybrid functional such as B3LYP [7, 8, 52, 62, 109] (Becke, three-parameter and Lee-Yang). It mixes exchange energies calculated in an exact (Hartree–Fock) manner with those obtained from DFT methods in order to improve the accuracy of the calculations. This exchange–correlation functional takes the form:

$$E_{xc}^{B3LYP} = aE_x^{HF} + (1-a)E_x^{LSDA} + bE_x^{B88} + cE_c^{LYP} + (1-c)E_c^{LSDA}, \quad (3.15)$$

where $a = 0.2$, $b = 0.72$, $c = 0.81$, chosen to fit the experimental data. Another important functional is called the Coulomb-attenuated hybrid exchange-correlation functional (CAM-B3LYP [111]). It has been frequently used in most of the works in this thesis to recover the effect of long range exchange (charge transfer) between electrons and nuclei. This long-range exchange functional has the form

$$\frac{1}{r_{ab}} = \frac{1-[\alpha+\beta\cdot erf(\mu r_{ab})]}{r_{ab}} + \frac{\alpha+\beta\cdot erf(\mu r_{ab})}{r_{ab}} \quad (3.16)$$

where $\alpha = 0.19$, $\beta = 0.46$, $\mu = 0.33$.

3.3 Vibronic theory

Before we start our discussion concerning resonance Raman scattering from a vibrational theory point of view, we clarify that our study in this section is based on the following assumptions:

- The Born-Oppenheimer approximation is allowed, meaning that the vibronic states $|r\rangle$ can be separated into products of electronic (Ψ) and vibrational (χ) wave functions:

$$|r(q,Q)\rangle = |\Psi(q,Q)|\chi(Q)\rangle \tag{3.17}$$

- The electronic transition dipole moment is expanded in a Taylor-series as a function of the normal coordinates Q:

$$\langle \chi_{\nu_s}\Psi_s|\hat{\mu}_\alpha|\chi_{i_0}\Psi_0\rangle = \langle \chi_{\nu_s}|\mu^{el}_{\alpha,s0}|\chi_{i_0}\rangle = \tag{3.18}$$

$$\mu^{el}_{\alpha,s0}\langle \chi_{\nu_s}|\chi_{i_0}\rangle + \sum_k \left[\frac{\partial \mu^{el}_{\alpha,s0}}{\partial Q_k}\right]_0 \langle \chi_{\nu_s}|Q_k|\chi_{i_0}\rangle + O(Q_k^2), \tag{3.19}$$

- The non-resonant term in the scattering amplitude of the cross section is neglected (only in resonance case),
- Only one excited electronic state is important $|s\rangle$, meaning that the incident light is in resonance with state $|s\rangle$,
- The electronic ground and excited-state potential energy surfaces are harmonic, and they have the same vibrational frequencies,
- Only FC-type contributions are important, meaning that the first order in Eq (3.18) (Herzberg-Teller) is neglected,
- For simplicity we consider here only the fundamental transitions ($|0\rangle \rightarrow |1\rangle$), but overtone and combination bands should be considered in some cases (see paper VII.)

3.3.1 Time-dependent resonance Raman scattering

The RRS theory is based on Kramers-Heisenber-Dirac formula of the transition polarizability tensor α which is derived from second-order perturbation theory [110]. For randomly oriented molecules the scattering cross-section from an initial vibrational state $|g,i\rangle = |0,0\rangle$ to a final vibrational state $|g,f\rangle = |0,f\rangle$ in the ground electronic state, is given by [72]

$$\sigma_{fi} = \frac{8\pi\omega_s^3\omega}{9c^4}\sum_{\alpha\beta}|[\alpha_{\alpha\beta}]_{fi}|^2, \tag{3.20}$$

where ω_s is the scattered angular frequency, c is the speed of light and ω is the angular frequency of the external electric field. The scattering tensor $[\alpha]_{fi}$ with components $[\alpha_{\alpha\beta}]_{fi}$ is defined as

$$[\alpha_{\alpha\beta}]_{fi} = \frac{1}{\hbar}\sum_{\nu_s}\left[\frac{\langle f|\hat{\mu}_\alpha|\nu_s\rangle\langle\nu_s|\hat{\mu}_\beta|0\rangle}{(\omega_s-\omega_g)+(\epsilon_{\nu_s}-\epsilon_0)-\omega-i\Gamma}\right], \tag{3.21}$$

where $\hat{\mu}_\alpha$ is the electric dipole operator along the molecular axis $\alpha = \{x, y, z\}$, Γ is the broadening of the excited state $|s\rangle$ and $\omega_s - \omega_g$ corresponds to the Bohr frequency of the transition ($|g, 0\rangle \rightarrow |s, 0\rangle$).

Since my objective in this section is to capture the physical features of RRS, and get further insights into its dynamical aspect, it becomes helpful to cast the two-photon events in a time domain formalism. The formula in Eq (3.21) describes a steady state of a two-photon event and has no explicit reference to time. On the other hand time-dependent theory affords an alternative description of this phenomenon and is therefore appropriate to address RRS.

The starting point of time-dependent RRS is to convert the scattering tensor expression in Eq (3.21) into a time-dependent formalism by using the half Fourier transform [72]

$$[\alpha_{\alpha\beta}]_{fi} = \frac{i}{\hbar}\int_0^\infty \sum_{\nu_s}\exp\{-i(\omega_s-\omega_g+\epsilon_{\nu_s}-\epsilon_0-\omega-i\Gamma)t\}\langle f|\hat{\mu}_\alpha|\nu_s\rangle\langle\nu_s|\hat{\mu}_\beta|0\rangle dt \tag{3.22}$$

and since

$$\exp\{-i(\omega_s+\epsilon_{\nu_s})t\}|\nu_s\rangle = \exp\{-i\hat{H}_s t/\hbar\}|\nu_s\rangle \tag{3.23}$$

where $\hat{H}_s$ is the Hamiltonian for nuclear motion on the electronic excited state potential surface $|s\rangle$. Further, if we plug Eq 3.23 into Eq 3.22 we will arrive at

$$[\alpha_{\alpha\beta}]_{fi} = \frac{i}{\hbar}\int_0^\infty dt\exp\{i(\omega_g+\epsilon_0+\omega+i\Gamma)t\}\langle f|(\hat{\mu}_\alpha)\exp\{-i(H_s)t/\hbar\}(\hat{\mu}_\beta)|0\rangle \tag{3.24}$$

where we have used $\sum_{\nu_s}|\nu_s\rangle\langle\nu_s| = 1$. Now let us make some interpretations of our new formula (Eq (3.24)). Fig. 3.1 shows clearly that the two-photon process begins from the initial vibrational state of the ground state $|0\rangle$ and is represented by a potential harmonic function. At time zero, interaction with the incident photon of energy $\hbar\omega$ causes a vertical transition to the electronic excited state potential surface. In this case the vibrational state $|0\rangle$ is now under the control of the Hamiltonian $\hat{H}_s$. Moreover, when the the Hamiltonian acts on the state $|0\rangle$, the wave packet starts to propagate on the surface ($\exp\{-i(H_s)t/\hbar\}(\hat{\mu}_\beta)|0\rangle = |0(t)\rangle$). The motion of the wave packet $|0(t)\rangle$ is determined by the displacement ΔQ between the ground and excited states potential. If the magnitude of ΔQ is significant, the wave packet $|0(t)\rangle$ will

move from its initial position to the right-hand side of the upper potential. It is then reflected and moves back to positions of shorter internuclear distances (Fig. 3.1). During this traveling process forth and back on the surface, the wave packet crosses a region where it overlaps with the wave function $|f\rangle$ in the ground state potential surface.

Now let us investigate the above mentioned situation by considering one cycle of vibration i.e. $0 \rightarrow 1 \rightarrow 2 \rightarrow 3 \rightarrow 4$ (see Fig. 3.1). The plot shows Raman overlap ($\langle f|i(t)\exp\{-\Gamma t/\hbar\}$) as a function of time. The overlap maximum value takes place in a very short time (a few picoseconds), after the start of propagation ($0 \rightarrow 1$). The points 0 and 1 correspond to the equilibrium separation in the ground state and internuclear separation (at maximum overlap), respectively. When the wave packet ($|0(t)\rangle$) continues to propagate and moves a way from the mentioned region (0 and 1), the Raman overlap decreases dramatically and reach its minimum at point 2 (see Fig. 3.1). It follows that the $|0(t)\rangle$ is then reflected back and the Raman overlap gradually increases again to reach its second highest value at point 3. Finally, one complete cycle of vibration ends at point 4, where the Raman overlap becomes zero, due to the orthogonality between $|0(t)\rangle$ and $|f\rangle$=$|1\rangle$. After a period of time $\hbar/\Gamma_s$, the oscillation process between these two turning points will be killed by the damping function $\exp\{-\Gamma t\}$ (see Fig. 3.1). A more general and deep description about such phenomena has been discussed in paper VII and [69, 53, 58, 110].

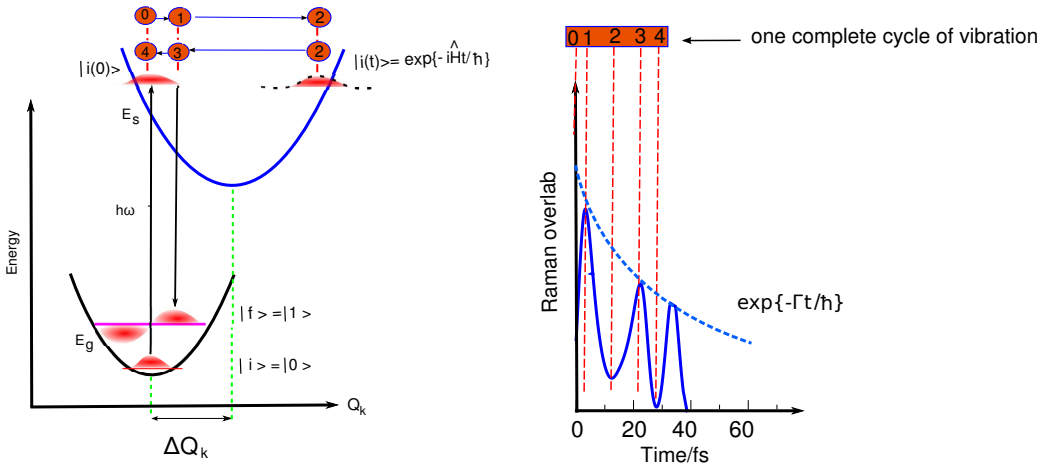

Figure 3.1: A pictorial representation of the wave-packet propagation and Raman overlap in the RRS process.

3.3.2 Linear coupling model (LCM)

We will discuss briefly how to calculate Franck–Condon (FC) factors by using the linear coupling model (LCM). The RRS intensity of the overtones and combination bands require several products of these factors. Furthermore, their integrals are known analytically in terms of the displacements Δ_k of the excited state equilibrium [73] (see Fig. 3.2). Based on our assumptions that has been indicated at the beginning of this section, the multi-mode FC amplitude:

$$\langle \chi_{s,\nu} | \chi_{g,i} \rangle = \prod_{k=1}^{3N-6} \langle m_k^{\nu} | n_k^{i} \rangle \tag{3.25}$$

where s is electronic excited state, g is the electronic ground state and k is the vibrational modes. The products of FC factors of the k:th mode are given by [18, 84, 83]

$$Y_i(\nu) = \langle 0|\nu\rangle\langle\nu|i\rangle \tag{3.26}$$

where $\langle 0|\nu\rangle$ is the overlap integral between the zero level of the ground state wave function and ν:th excited state wave function, and $\langle\nu|i\rangle$ is related to the integral for transition back to i:th level of the ground state (see Fig. 3.2). The values of $Y_i(\nu)$ for i=0, 1, 2, 3 are given by [18]

$$Y_0(\nu_k) = \left(\frac{\Delta_k^{2\nu_k}}{2^{\nu_k}\nu_k!}\right) \exp\left(\frac{-\Delta_k^2}{2}\right), \tag{3.27}$$

$$Y_1(\nu_k) = Y_0(\nu_k)\frac{\left(\Delta_k - \frac{2\nu_k}{\Delta_k}\right)}{\sqrt{2}}, \tag{3.28}$$

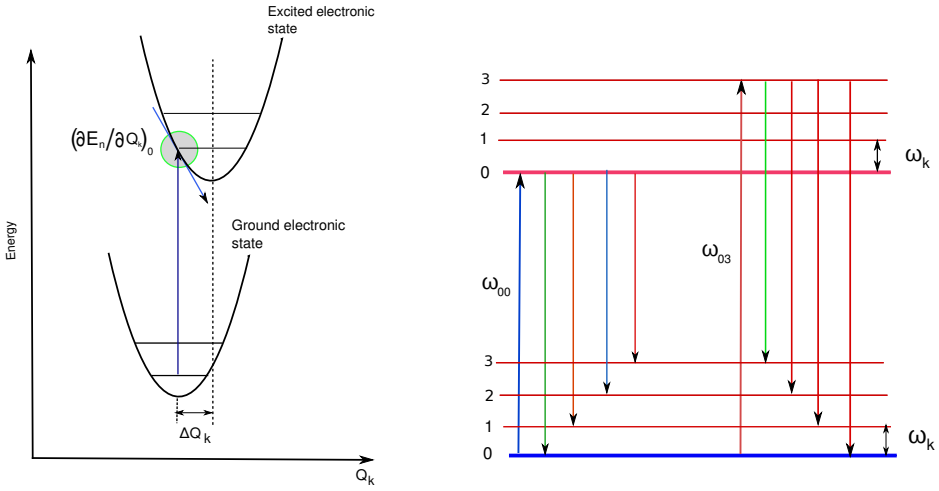

Figure 3.2: The gradient of the excited state along a normal coordinate Q, and the resonance Raman energy level diagram shows the transitions and scattering process of the initial and final states.

$$Y_2(\nu_k) = Y_0(\nu_k)\frac{(\Delta_k^2 - 4\nu_k + \frac{4\nu_k(\nu_k-1)}{\Delta_k^2})}{2\sqrt{2}}, \tag{3.29}$$

$$Y_3(\nu_k) = Y_0(\nu_k)\frac{(\Delta_k^3 - 6\nu_k\Delta_k + \frac{12\Delta_k(\Delta_k-1)}{\Delta_k} - \frac{8\nu_k(\nu_k-1)(\nu_k-2)}{\Delta_k^3})}{4\sqrt{3}}, \tag{3.30}$$

where Δ_k is the dimensionless shift parameter:

$$\Delta_k = -\frac{1}{\sqrt{2\hbar\omega_k^3}}\left(\frac{\partial E^e}{\partial Q_k}\right)_0 \tag{3.31}$$

Further, the partial derivatives of the excited state potential surface with respect to nuclear displacements are determined at the equilibrium geometry:

$$\frac{\partial E^e}{\partial Q_k} = \frac{E^e(R_{eq}^g + \frac{\delta Q_k}{\sqrt{\text{amu}}}) - E^e(R_{eq}^g - \frac{\delta Q_k}{\sqrt{\text{amu}}})}{2|\delta|} \tag{3.32}$$

where R_{eq}^g (in a.u.) is the ground state Cartesian coordinate. The numerical differentiations are performed along the normal vibrational coordinates Q_k (in a.u.$\times\sqrt{\text{amu}}$) with step lengths $\delta = 0.01 \times \sqrt{\text{amu}}$ (in a.u.), where amu = 1822.8884843 (see Fig. 3.2).

Vibrational normal coordinates

Assume that we want to investigate the internal motion of a molecule that consists of N atoms. It is natural to think that we need $3N$ coordinates to describe the degrees of freedom of the N atoms in three dimensions. These coordinates include the translation of the center of the mass of the molecule and three (or two) angles to specify the rotation of the nonlinear (or linear) molecule as a whole about its mass center [60, 32]. So the motion of the molecule can be splitted into three parts, namely, vibration, translation and rotation [98]. The last two parts are eliminated when we use the internal coordinates to describe the internal motion of the molecule. Consequently, we will have $3N-6$ (or $3N-5$) coordinates to describe the vibration of the molecule. All the atoms will in principle participate in the vibrations (motions) of the molecule and their vibrational energies transferred to each other. In this case the molecular potential energy is depending on the displacements of the atoms from their equilibrium positions. When the displacements Δq_i are small ($\Delta q_i = q_i - q_{i0}$), we can express the molecular potential energy in a second-order Taylor expansion around the equilibrium positions as [42, 6]

$$V = V(q_{01}, \cdots, q_{0N}) + \sum_{i}^{3N} \left(\frac{\partial V}{\partial q_i}\right)_0 \Delta q_i + \frac{1}{2} \sum_{i,j}^{3N} \left(\frac{\partial^2 V}{\partial q_i \partial q_j}\right)_0 \Delta q_i \Delta q_j + \cdots \quad (3.33)$$

We have used so called mass-weighted coordinates $q_i = m_i^{1/2} x_i$ where, m_i is the mass of the atom that is displaced by x_i. The first term in the series (3.33) is the potential energy of the equilibrium position, and this may be made to vanish by shifting the arbitrary zero of the potential to coincide with the equilibrium potential. Furthermore the second term which is linear in Δq_i is also vanishing, due to the equilibrium conditions (the acting force on the molecule vanishes $F_i = -\left(\frac{\partial V}{\partial q_i}\right)_0 = 0$). We are therefore ending up with the quadratic terms and the first approximation to the molecular potential V becomes

$$V = \frac{1}{2} \sum_{i,j}^{3N} \left(\frac{\partial^2 V}{\partial q_i \partial q_j}\right)_0 \Delta q_i \Delta q_j \quad (3.34)$$

where $\left(\frac{\partial^2 V}{\partial q_i \partial q_j}\right)_0$ is the the Hessian or known as force constant. The partial derivatives with respect to q_i, q_j describe the case where a displacement of one atom may influence the restoring force experienced by another. Although, the introduction of the mass-weighted coordinates q_i simplify the problem of the coordinates ($T = \frac{1}{2} \sum_i^{3N} m_i \dot{x}_i^2$), we still have another problem concerning the separation of modes due to the cross-terms in the potential when $i \neq j$. To overcome this problem we define a new set of coordinates Q_k called normal

coordinates and express them as a linear combination of the q_i:

$$Q_k = \sum_i^{3N} L_{ik} q_i \tag{3.35}$$

where L_{ik} is the matrix of eigenvectors of the Hessian. Each normal mode gives rise to an oscillating dipole of angular frequency ω_k. The kinetic and the potential energy can be expressed in the normal coordinates Q_k:

$$T = \frac{1}{2} \sum_i^{3N} \dot{Q}_k^2 \quad , V = \frac{1}{2} \sum_i^{3N} \omega_i^2 Q_i^2 \tag{3.36}$$

Infrared absorption (IR)

Infrared spectroscopy (IR) is dealing with electromagnetic radiation in the infrared region with a wavelength between 0.7–300 μm, that is longer than the wavelength of visible light (390–750 nm). If the IR incident radiation interacts with a molecule with vibrational frequency ω_ν and if the radiant energy matches the molecule vibrational energy, then the radiation will be absorbed. The absorption will in turn change the molecular vibrational amplitude. The molar absorption coefficient $\varepsilon(\nu)$ can be written as a function of the wavenumber ν (in cm^{-1}):

$$\varepsilon(\nu) = \frac{1}{CD} \log_{10}(\frac{I_0(\nu)}{I(\nu)}) \tag{3.37}$$

where C is the absorbers concentration (in mol L^{-1}), D is the length of the optical path through the absorber (in cm), I is the intensity of the incident light at frequency ω, and I_0 is intensity of the transmitted light at the same frequency (ω). If we integrate the absorption coefficient $\varepsilon(\nu)$ in Eq. 3.37 over the entire absorption band we will end up with

$$A_k = \int \varepsilon(\nu) d\nu \tag{3.38}$$

where A_k represents the transition intensity (in cm^{-2} L mol^{-1}). A_k can also be approximated by [36]

$$A_k \propto |\frac{\partial \mu}{\partial Q_k}|^2 \tag{3.39}$$

where $\frac{\partial \mu}{\partial Q_k}$ is the partial derivative of the dipole-moment along the normal coordinates Q_k. Eq. 3.39 can be compared to the Raman intensity:

$$I_k \propto |\frac{\partial \alpha}{\partial Q_k}|^2 \tag{3.40}$$

3.4 Response theory

In section (3.3), I presented shortly the vibronic theory and focused on resonance Raman scattering (RRS) from a time-dependent point of view. This section will be devoted to response theory and the investigation of Raman scattering when the strength of the electric field is varied between low and high intensity. Depending on the strength of the electric field the response of the medium can be linear (low intensity) or non-linear (high intensity) [76, 75, 79].

The starting point of linear scattering is the motion of charges to first order in term of the linear electric polarizability tensor ($\alpha_{\alpha\beta}(\omega)$). When the strength of the electric field (E^{ω}) is weak, the perturbation of the electron cloud causes a periodic separation of the charges within the molecule which gives rise to an induced dipole moment ($\hat{\mu}^{ind} = \alpha_{\alpha\beta}E^{\omega}_{\beta}$). The periodic charge separation depends also on the frequency (ω) of the electric field and thus the polarizabilty becomes frequency dependent as well:

$$\mu_{\alpha}(t) = \mu^{0}_{\alpha} + \sum_{\omega} \alpha_{\alpha\beta}(-\omega;\omega)E^{\omega}_{\beta}e^{-i\omega t} \tag{3.41}$$

where μ^{0}_{α} is the permanent electric dipole moment and E^{ω}_{α} are the Fourier amplitudes of the electric field along the molecular axis α. Due to hermiticity, we may without loss of generality assume that the amplitudes of the electric field are real $E^{-\omega} = (E^{-\omega})^{*}$. We notice here that the summation includes both the positive and negative frequencies.

Now let us consider the case when the strength of the electric field (E^{ω}) is strong enough to cause nonlinear light-matter interactions. In this situation we will express the time-dependent polarization (Eq. 3.41) as a perturbation expansion according to [77]

$$\begin{aligned}\mu_{\alpha}(t) &= \mu^{0}_{\alpha} + \sum_{\omega} \alpha_{\alpha\beta}(-\omega;\omega)E^{\omega}_{\beta}e^{-i\omega t} \\ &+ \frac{1}{2}\sum_{\omega_1,\omega_2} \beta_{\alpha\beta\gamma}(-\omega_{\sigma};\omega_1,\omega_2)E^{\omega_1}_{\beta}E^{\omega_2}_{\gamma}e^{-i\omega_1+\omega_2 t} \\ &+ \frac{1}{6}\sum_{\omega_1,\omega_2,\omega_3} \gamma_{\alpha\beta\gamma\delta}(-\omega_{\sigma};\omega_1,\omega_2,\omega_3) \times E^{\omega_1}_{\beta}E^{\omega_2}_{\gamma}E^{\omega_3}_{\delta}e^{-i\omega_1+\omega_2+\omega_3 t}\end{aligned} \tag{3.42}$$

where $\alpha_{\alpha\beta}(-\omega;\omega)$, $\beta(-\omega_{\sigma};\omega_1,\omega_2)$ and $\gamma(-\omega_{\sigma};\omega_1,\omega_2,\omega_3)$ are the linear polarizability, first-order and the second-order hyperpolarizability, respectively. It is worthwhile to notice that just as in the linear polarizability case, the nonlinear coupling constants, namely β and γ depend on the frequency of the applied electric field. Furthermore, the nonlinear terms in Eq. 3.42 are usually small compared to the linear term α which, for instance, gives rise to linear Raman scattering. However, the contribution from nonlinearty terms β and γ become sufficiently intense to be detected when the applied electric field is

"large" (Q-switched laser) [47]. When the intensity of the applied field is high, the density of photons becomes high as well and in turn increases the probability for multi-photon interactions with an individual molecule. Coherent anti-Stokes Raman scattering (CARS) and hyper Raman scattering (HRS) are two different techniques based on nonlinear optics which are also known as second-harmonic generation, and treated in this thesis.

3.4.1 Resonance Raman scattering (RRS) from the derivative of the polarizability tensor

In the previous section, we have referred to the linear polarizability tensor $\alpha_{\alpha\beta}(-\omega;\omega)$ and mentioned that one can use this expression to calculate Raman scattering. The normal Raman scattering can be calculated by applying the Placzek theory of polarizability tensor and this has been treated in detail in Ref. [58]. In this section we will use an approximate method to calculate resonance Raman scattering by using a complex polarization propagator (CPP) approach. A detailed derivation of the expression of the α tensor, including the solution of the linear response function can be found in a work by Norman *et al* [76]. In order to determine Raman scattering cross section from first principles, we need at the molecular level to determine the values of the electric-dipole polarizability in the resonant regions of the spectrum (as detailed in paper II [64]). The resonant convergent sum-over-states expression for the polarizability reads [80]

$$\alpha_{\alpha\beta}(-\omega;\omega) = \frac{1}{\hbar}\sum_{n>0}\left[\frac{\langle 0|\hat{\mu}_\alpha|n\rangle\langle n|\hat{\mu}^\omega_\beta|0\rangle}{\omega_n-\omega-i\Gamma/2} + \frac{\langle 0|\hat{\mu}^\omega_\alpha|n\rangle\langle n|\hat{\mu}_\beta|0\rangle}{\omega_n+\omega+i\Gamma/2}\right], \tag{3.43}$$

where $\hat{\mu}_\alpha$ is the electric dipole operator along the molecular axis $\alpha = \{x,y,z\}$, $\hbar\omega_n$ is the excitation energy, Γ_n is the broadening of excited state $|n\rangle$, and, ω is the angular frequency of the external electric field. The Raman scattering cross section is given by [54]

$$\sigma^{fi}_{\alpha\beta} \propto |\langle f,g|\alpha_{\alpha\beta}|i,g\rangle|^2 \tag{3.44}$$

where $\langle f,g|$ and $|i,g\rangle$ is the initial and final vibrational state of the ground state g. Let us now consider the RRS cross section for the fundamental 0→1 transition and apply the two-state model approximation close to resonance. In this case the second term in Eq. (3.43) is very small relative to the first term. Further, we use perturbation theory and expand the geometry dependence of the electronic polarizability in Eq. 3.43 in a Taylor series with respect to the normal coordinates Q_a

$$\alpha_{\alpha\beta}\left(Q_1,Q_2,\ldots Q_N\right) = \alpha^0_{\alpha\beta} + \sum_a \frac{\partial\alpha_{\alpha\beta}}{\partial Q_a}Q_a + \ldots. \tag{3.45}$$

We can therefore, based on Eq. (3.43), determine the necessary derivatives of $\alpha_{\alpha\beta}$ with respect to normal coordinate Q_a of mode a by means of numerical differentiation and regarding the transition dipole moment to be independent of Q_a.

$$\frac{\partial \alpha_{\alpha\beta}}{\partial Q_a} = -\frac{\langle 0|\hat{\mu}_\alpha|1\rangle\langle 1|\hat{\mu}_\beta|0\rangle}{(\omega_{10} - \omega - i\Gamma/2)^2} \cdot \frac{\partial \omega_{10}}{\partial Q_a} \tag{3.46}$$

It is clear that the value of the polarizability is largely dictated by the position of the excitation energy, and, consequently, $\partial\alpha/\partial Q$ is tightly linked to the gradient of the excitation energy ($\partial\omega_e/\partial Q$). The gradient of the potential surface of the excited state can be evaluated using two point numerical differentiation (see Eq. 3.32). Returning to Eq. (3.44) and keeping only the leading order non-vanishing term in the expansion of the polarizability, we obtain the following expression for the RRS cross section

$$\sigma^{10}_{\alpha\beta} \propto \left(\frac{\partial E^e}{\partial Q_a}\right)^2_0 \cdot \left(\frac{\mu}{\Gamma}\right)^4 \cdot \frac{1}{\omega_a} \tag{3.47}$$

where $\langle 1|Q|0\rangle = \sqrt{\frac{\hbar}{2\omega_a}}$ is evaluated according to simple harmonic oscillators approximation. Eq. (3.47) shows clearly that the RRS cross section is scaled by $\frac{1}{\Gamma^4}$ and this might overestimate the cross section value compared with the vibronic theory calculation (see paper VII) [46, 50].

Oscillator strength and absorption cross section

The linear polarizability tensor in Eq. (3.43) can also be used to calculate the oscillator strength f_{n0} $(0 \rightarrow n)$ and light absorption cross section σ of a system by considering the imaginary part of $\alpha_{\alpha\beta}(-\omega;\omega)$ [13, 77, 43], which can be written as

$$\alpha_{\alpha\beta}(-\omega;\omega) = \alpha^{Re}_{\alpha\beta}(-\omega;\omega) + i\alpha^{Im}_{\alpha\beta}(-\omega;\omega) \tag{3.48}$$

The real part $\alpha^{Re}_{\alpha\beta}$ of the polarizability tensor is associated with the refractive index of the system and the imaginary part $\alpha^{Im}_{\alpha\beta}$ with the light absorption cross section. The absorption cross section σ can be regarded as the effective region of the system for removing radiation from an incident light and is given by [77]

$$\sigma(\omega) = \frac{4\pi\omega}{c}\bar{\alpha}^{Im}_{\alpha\beta}(-\omega;\omega) \tag{3.49}$$

where c and is the speed of light and $\bar{\alpha}^{Im}_{\alpha\beta}(-\omega;\omega)$ is the isotropic average of the polarizability:

$$\bar{\alpha} = \frac{1}{3}\sum_{\alpha=x,y,z} \alpha_{\alpha\alpha} \tag{3.50}$$

Now let us consider the resonance term of $\alpha^{Im}_{\alpha\beta}(-\omega;\omega)$ which is given by [77]

$$\frac{\Gamma}{2\hbar}\sum_{n>0}\frac{\langle 0|\hat{\mu}_\alpha|n\rangle\langle n|\hat{\mu}^{\omega}_{\beta}|0\rangle}{(\omega_n-\omega)^2+(\Gamma/2)^2} \tag{3.51}$$

If we insert Eq. (3.51) in Eq. (3.49), and let $\Gamma \to 0$ we will end up with

$$\lim_{\Gamma\to 0}\sigma(\omega)=\frac{4\pi^2\omega}{3\hbar c}\sum_{n>0}\{\delta(\omega_n-\omega)\sum_{\alpha}|\langle 0|\mu_\alpha|n\rangle|^2\} \tag{3.52}$$

where $\delta(\omega_n-\omega)$ is Dirac-delta function. Now it becomes clear that the oscillator strengths ($f_{n0}=\frac{2\omega|\mu_{na}|^2}{3}$ in atomic unit) are connected with the lifetime $\Gamma = 1/\tau$ approximation of light absorption from the imaginary part of the linear polarizability.

3.4.2 Coherent anti-Stokes Raman scattering (CARS)

My purpose in this section is not to give a complete derivation of the CARS theory, but only an outline of the formalism that is used in paper III for calculations of CARS spectra [65]. As mentioned in section 2.3.1 the Coherent anti-Stokes Raman Scattering (CARS) phenomenon is based on a four-wave mixing process in which two of the incoming laser frequencies are identical [68] (see Fig. 2.4). The outcome of this mixing process is an observed CARS signal that associates with the non-linear fourth-order susceptibility tensor $\chi^{(3)}(-\omega_\sigma;\omega_p,-\omega_s,\omega_p)$, where the negative sign of the frequency ω_s corresponds to a deexcitation (the Stokes signal). The outgoing CARS signal is given as $\omega_\sigma = 2\omega_p - \omega_s$. In a molecule, the susceptibility tensor is governed by the non-linear second-order hyperpolarizability tensor γ (see paper III) [78, 65, 105]. Furthermore, the dominating CARS signal arises when the frequency difference $\omega_p - \omega_s$ is tuned to a vibrational excitation in the molecule $\omega_{\nu 0}$. In this case, the CARS process has in principle the same information content as conventional normal Raman scattering, but with a much higher intensity (see paper III) [65]. Moreover, the resonant CARS signal is given by [68, 105, 65]

$$\begin{aligned}\gamma^{\mathrm{CARS,Res}}_{\alpha\beta\gamma\delta}(-\omega_\sigma;\omega_p,-\omega_s,\omega_p) \;\approx\; & \frac{2}{\hbar}\sum_{\nu}\left[\frac{\langle 0\,|\alpha_{\alpha\beta}(\omega_p)|\,\nu\rangle\,\langle\nu\,|\alpha_{\gamma\delta}(\omega_p)|\,0\rangle}{\omega_{\nu 0}-(\omega_p-\omega_s)+i2\varepsilon}\right. \\ & + \left.\frac{\langle 0\,|\alpha_{\alpha\delta}(\omega_p)|\,\nu\rangle\,\langle\nu\,|\alpha_{\gamma\beta}(\omega_p)|\,0\rangle}{\omega_{\nu 0}+(\omega_p-\omega_s)+i2\varepsilon}\right],\end{aligned} \tag{3.53}$$

where the summation runs over all the excited vibrational states ν of the electronic ground state of the molecule and $\alpha_{\alpha\beta}(\omega)$ is the frequency-dependent electronic polarizability as in Eq. 3.43, but with $\Gamma = 0$. Furthermore, we use Eq. 3.45 and represent the vibrational eigenstates as harmonic oscillators, and

keeping only the leading order non-vanishing term in the expansion of the polarizability, we obtain the following expression for the resonant contribution to the CARS intensity:

$$\begin{aligned}&\gamma_{\alpha\beta\gamma\delta}^{CARS,Res}\left(-\omega_\sigma;\omega_p,-\omega_s,\omega_p\right)\approx\\&\frac{2}{\hbar}\sum_a\left\{\left(\frac{\partial\alpha_{\alpha\beta}\left(\omega_p\right)}{\partial Q_a}\right)\left(\frac{\partial\alpha_{\gamma\delta}\left(\omega_p\right)}{\partial Q_a}\right)\left[\omega_{\nu 0}-\left(\omega_p-\omega_s\right)+i2\varepsilon\right]^{-1}\right.\\&\left.+\left(\frac{\partial\alpha_{\alpha\delta}\left(\omega_p\right)}{\partial Q_a}\right)\left(\frac{\partial\alpha_{\gamma\beta}\left(\omega_p\right)}{\partial Q_a}\right)\left[\omega_{\nu 0}+\left(\omega_p-\omega_s\right)+i2\varepsilon\right]^{-1}\right\}\end{aligned}\tag{3.54}$$

The final expression for the CARS signal can be obtained by specifying the real and imaginary parts of the γ tensor in Eq. (3.54) as γ_ν^R and γ_ν^I respectively and the electronic second hyperpolarizability as γ_e.

$$|\gamma|^2=(\gamma_\nu^R+\gamma_e)^2+\gamma_\nu^I\tag{3.55}$$

where we have performed an isotropic averaging of the γ tensor:

$$\gamma=\frac{1}{15}(\gamma_{\zeta\eta\eta\zeta}+\gamma_{\zeta\eta\zeta\eta}+\gamma_{\zeta\zeta\eta\eta}),\tag{3.56}$$

3.4.3 Hyper Raman scattering (HRS)

As we mentioned in section (2.4), the HRS signal I(ω_s) is generated due to non-linear three photon process and associated with the first-order hyperpolarizability tensor β. Furthermore, applying the Born-Oppenheimer approximation, the expression for the Stokes hyper-Raman intensity is given as [86, 87, 88]

$$I(\omega_s)\propto(\omega_s)^4|\langle i|\beta(\omega,Q)|f\rangle|^2,\tag{3.57}$$

where ω_s is the scattered frequency, $\langle i|$ and $|f\rangle$ are the initial and final vibrational states of the ground state, and $\beta(\omega,Q)$ is the expectation value of the hyperpolarizability. The scattered frequency ω_s is created when a single incident light with two identical frequencies ω coincide with the vibrational frequency of the molecule ω_ν, such that [71] $\omega_s=2\omega-\omega_\nu$ (see Fig. 2.1).

In order to evaluate the expressions in Eq. (3.57), the vibrational potential and hyperpolarizability can be expanded in a Taylor series over the normal modes Q [9, 10, 11], so that

$$\begin{aligned}\beta_{\alpha\beta\gamma}(Q)=&\beta_{\alpha\beta\gamma}^0+\sum_i\left(\frac{\partial\beta_{\alpha\beta\gamma}}{\partial Q_i}Q_i+\frac{1}{2}\sum_j\left(\frac{\partial^2\beta_{\alpha\beta\gamma}}{\partial Q_i\partial Q_j}Q_iQ_j+\right.\right.\\&\left.\left.\frac{1}{6}\sum_k\frac{\partial^3\beta_{\alpha\beta\gamma}}{\partial Q_i\partial Q_j\partial Q_k}Q_iQ_jQ_k+\cdots\right)\right)\end{aligned}\tag{3.58}$$

where Greek subscripts denote Cartesian axes, and

$$V(Q) = V^{(0)} + \sum_i \left(V_i^{(1)} Q_i + \frac{1}{2} \sum_b \left(V_{ij}^{(2)} Q_i Q_j + \frac{1}{6} \sum_k V_{ijk}^{(3)} Q_i Q_j Q_k + \cdots \right) \right), \tag{3.59}$$

where $V_{i\cdots}^{(r)}$ denotes the r th order derivative of the energy at the expansion point with respect to normal coordinates.

A common approximation, adopted in the present work, is the so-called double harmonic approximation [86], wherein the expansions for β and V are truncated after the first and second derivatives, respectively. In the double-harmonic approximation, the vibrational wave functions are harmonic oscillators, and applying Eq. 3.58 and Eq. 3.59 to Eq. 3.57 yields

$$I(\omega_s) \propto (2\omega - \omega_\nu)^4 |\langle i| \left(\frac{\partial \beta(-2\omega; \omega, \omega)}{\partial Q_\nu} \right)_0 Q_\nu |f\rangle|^2, \tag{3.60}$$

The subscript zero for the derivative $\frac{\partial \beta}{\partial Q_t}$ means that the derivative is evaluated at the equilibrium geometry (for more detail see paper VI).

Chapter 4

Applications of linear and nonlinear Raman scattering

In this chapter, I illustrate, using my own research results, some examples of the wide applicability of linear and non-linear Raman spectroscopy, both with regard to the nature of the samples that can be investigated and the information that can be provided.

4.1 Linear Raman scattering

4.1.1 Stand-off detection of explosive substances

Raman spectroscopy has in general widespread applications in study of physical, chemical, medical and biological systems. Such applications vary from qualitative information to highly quantitative results. For instance Raman spectra are often used to identify different chemical species, due to the fact that each different scattering molecule gives its own characteristic fingerprint in the spectrum. In such cases, changes in wavenumber and intensity of the spectra may be used to investigate relaxation phenomena and the effect of environment, temperature and pressure on the chemical species [58]. Vibrational Raman intensities may also be used to measure the concentration of the scattering species [57].

The potential applications of Raman spectroscopy was greatly promoted by the introduction of laser techniques and, later, the availability of photoelectric detection. The consequence of these developments is that now the Raman spectrum of almost any kind of material may be obtained under different physical conditions. There is no need nowadays for the material under study to be of good optical quality or virtually colorless, as very tiny quantities at ultra-low concentrations can be detected and even the small wavenumber shifts is unlikely to escape detection. Also, the development of tunable lasers has enabled studies

of Raman scattering under resonance conditions. In resonance Raman scattering (RRS), the energy of the incoming laser is adjusted such that it coincides with an electronic transition of the molecule. In this case, the intensity of the RRS becomes many orders of magnitude greater than normal Raman scattering (NRS) and the shape of the spectrum may become different. Furthermore, overtones as well as new bands may also be observed with appreciable intensity. This advanced technique has in turn opened up many new applications of Raman spectroscopy. For example, investigations of a wide range of problems in biological and medical systems have become possible. Another important application of Raman spectroscopy is the use of RRS for stand-off detection of gaseous samples at ultra-low concentrations. In such applications, the Raman spectra function as fingerprints of the explored samples. The use of resonant conditions implies an all-over increase of the intensity of the signal by several orders of magnitude and gives the possibility to improve the accuracy in the identification process by considering the diversity of the fingerprints obtained at the different resonances [63, 64].

To illustrate the application of such a technique we have studied in this thesis work an explosive molecules in gas phase and compared the results with the experimental data measured in solution as well as in crystalline solid [12]. Calculations of this kind includes first an optimization of the ground state geometry, which ideally should be carried out at the same level of theory as the actual spectral calculations. For larger systems and for analysis it is helpful to impose full point group symmetry that is associated with the optimized geometry. Considerations of parametrization in terms of exchange-correlation functionals, see e.g. [8, 52, 62, 109], and basis set, is important. Basis sets can form hierarchies in terms of accuracy, while density functionals in general do not. Experience and other type of calculations are often helpful to validate the parametrization before calculations are carried out. A posteriori validation is also of concern of course, when possible, and always forms a necessary (albeit not sufficient) criterion for the calculation in terms of chosen theoretical method and parametrization. It could be that a control via *ab initio* explicitly correlated methods, like the hierarchical coupled cluster method, becomes a necessary measure to fully establish the parameter choice in the chosen density functional technique.

Taking 2,4-dinitrotoluene (2,4-DNT) as an explicit example, we show, Fig. 4.1 (A), an experimental UV spectrum for this molecule in acentonitrile solution recorded by FOI (Swedish Defence Research Agency) [25]. The spectrum is dominated by two broad structureless absorption peaks with a maximum around 250 nm and a comparatively strong shoulder to the left of the main peak around 200 nm. We have included the experimental spectrum in Fig. 4.1 (A) for comparison with the theoretical one that is obtained in the present work. In the presentation of the theoretical spectrum, we have included bars to represent the calculated oscillator strengths and used a line profile obtained by an application of a Gaussian line broadening. From the theoretical spectrum, we

see two bands, due to electronic states namely $3\,^1A'$ and $6\,^1A'$, positioned at the transition wavelengths of 232 and 200 nm, respectively. Additionally, the peaks at 223, 246 and 263 nm are attributed to single electronic states, namely $4\,^1A'$, $2\,^1A'$ and $1\,^1A'$. The theoretically predicted absorption is in close agreement with the experimental one. For this molecule of charge-transfer character, we can attribute the quality of the theoretical calculation to the treatment of hole-electron Coulomb interactions in the CAM-B3LYP exchange-correlation functional. The experimental Raman spectra for 2,4-DNT in gas phase (RRS @ 248 nm) [25] and crystal (RRS @ 244 and NRS @ 785 nm) [12] have been measured by FOI [25] and Balnco *et al* [12], respectively, covering the wavenumbers between 1000 and 1800 cm^{-1}. For comparison, we include the (RRS @ 244 and NRS @ 785 nm) given in Ref. [12] as an inset of Fig. 4.1 (B). The NRS spectrum of DNT (crystal) consists of a medium intensive peak around 1600 cm^{-1} (Peak 1), a high intensity peak at 1353 cm^{-1} (Peak 3), two low intensive double peaks and one low intensity peak around 1550 (Peak 2), 1150 (Peak 5) and 1200 cm^{-1} (Peak 4), respectively. When the excitation frequency is tuned to 244 nm, the positions of the spectra features remain the same, while the shape of the peaks become slightly different in some part of the spectrum (see the inset in Fig. 4.1 (B)). The main difference between them is that the double peak around 1550 (Peak 2) and 1150 cm^{-1} (Peak 5) becomes a broad single peak, respectively. In the same figure we have also included the experimental spectrum for RRS at excitation wavelength of 248 nm (in gas phase). This spectrum consists of a strong intensive peak at 1353 cm^{-1} and a medium intensive peak at 1610 cm^{-1}, as in the case of the RRS spectrum at 244 nm. However, due to the background effect, the other peaks (Peak 5, 4 and 2) become unidentified. Our theoretical resonant Raman spectrum, which is obtained for the excited state $2\,^1A'$ at 246 nm (see Fig. 4.1, B), shows one intensive peak at 1353 cm^{-1} of the 4-N-$C_{arom.}$ symmetric stretch, a relatively medium intensity peak at 1620 cm^{-1} of the 2-N=O symmetric stretch and three small peaks around 1200 cm^{-1}. With respect to the prediction of intensities and positions for the same peaks (1, 2, 3, 4 and 5), the agreement between the theoretical and experimental spectra is compelling. It is clear that, with applications of stand-off detection in mind, the molecular fingerprint might change quite dramatically when the laser wavelength is tuned from one electronic resonance to another.

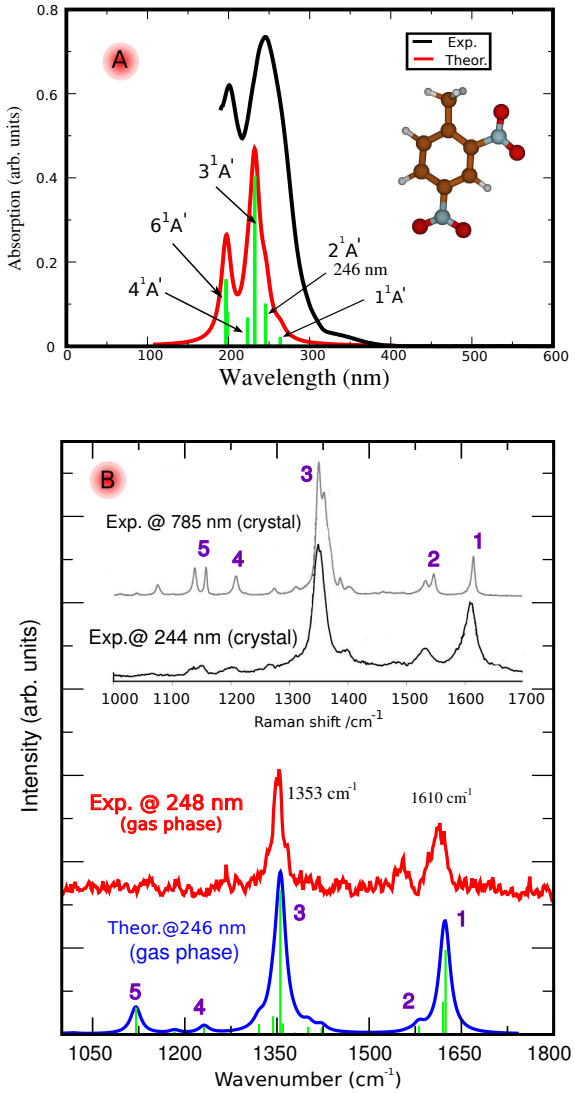

Figure 4.1: (A) UV absorption spectra for DNT calculated in gas phase and measured in solution with acentonitrile. The theoretical spectrum is based on the electronic oscillator strength distribution, broadened by Gaussian line profiles. (B) Resonant spectra at excitation wave length (Exp. 248 nm, Theor. 246 nm). The experimental spectrum is measured by the Swedish Defence Research Agency (FOI) in gas phase, using a long-pass filter cutting at 248 nm, the temperature was 359 K and vapor pressure 0.15 Torr. The inset shows experimental nonresonant (@ 785 nm) and resonant (@ 244 nm) Raman spectra for 2,4-DNT crystals, which is taken from Ref. [12].

4.1.2 Applications of RRS to Biomolecules

In the previous section we have reviewed the applicability of resonance and non resonance Raman spectroscopy as stand off detection of an explosive molecule namely 2,4-DNT. In this section we will present another important application of RRS, that is for biomolecules. Although the application of Resonance Raman scattering (RRS) in medicine and biology is aggravated by the presence of a fluorescence background, it has shown a promising capability to provide scientists with essential information concerning phenomena like drug-protein interactions, drug location and concentration in subcellular regions [20, 51, 99]. For instance, deoxyribonucleic acid (DNA) in water can be studied by the RRS techniques with relative ease [27] due to the fact that water shows a weak and structureless spectrum in Raman in contrast to its strong infrared absorption [17]. The individual as well as paired DNA bases such as denine-thymine and guanine-cytosine (with short excited state lifetimes of around 1 ps [2]), can also be investigated by this technique. Another promising application of RRS is the implementation and practical use of a novel photonic system based on the Raman effect for biomolecular detection. It implements stand-off in-vivo laser detection through the skin and the system will provide unique possibilities for non-invasive identification and quantitative measurement of biomolecules in blood and tissue [5].

To illustrate some of above mentioned applications of RRS in biology, we have analysed the RRS spectra of Trans-1,3,5-hexatriene (THT) and the Watson–Crick base pairs DNA, methylguanine-methylcytosine (MG-MC) and compared the results with the available experimental data. Trans-1,3,5-hexatriene (THT) is a linear polyene that has an important role a model system in photobiology such as for the retinal chromophore and the triene chromophores in vitamin D. It has also been found that hexatriene exhibits a vibronically well-resolved absorption spectrum and nonfluorescent properties. In addition to its small size those attributions make this molecule accessible to theoretical treatments as well as experimental investigations. The theoretical calculation based on the linear coupling model (LCM) which has been described in section (3.3.2). It is also relevant, as an actual example, to illustrate the considerations for the electronic structure theory to be used for the molecular property calculations. The adiabatic DFT level of theory made use of the correlation consistent basis sets [24]. Force fields are determined with use of a hybrid (here Coulomb attenuated) exchange-correlation functional [8, 52, 62, 109] in conjunction with the double-ζ basis set which shows high level of reliability and accuracy in frequency calculations in general [64, 63, 65, 66]. The calculations of excitation energies in general require a more extensive basis set, in this example a double-augmented basis set (d-aug-cc-pVTZ). For experimental comparison we need to employ a common broadening function for the excited states (here chosen equal $\gamma = 65.0\ \mathrm{cm}^{-1}$). This line width function is often not known a priori and poses also a considerable problem for *ab initio* computation.

For comparison, we include the experimental [70] and theoretical absorption spectra of THT in the upper panel of Fig. (4.2). The experimental spectrum has also been blue shifted about 6 nm to fit with the calculated spectrum. The prediction of the relative absorption intensities for the same peaks shows a compelling overall agreement between the two spectra. We note that, just as in the experimental spectrum, there are two dominant bands around 257 and 246 nm as a result of 0–0 and 0–1 transitions, respectively. The latter corresponds to a symmetric mode ν_5 (C=C) which contributes strongly to the absorption spectrum. There are also one predicted medium strong band around 249 nm (symmetric mode ν_{10}, =C–H) due to the 0–1 transition, two medium bands around 249 nm (mode $(\nu_5 + \nu_{10})$) and 237 nm (mode $2\nu_5$). By considering the FC factors, that is fundamental, combination and overtone (first and second) FC factors, it becomes very clear that the overtone and combination FC factors have a significant contribution to the spectra (see upper Fig. (4.2)).

The experimental resonance Raman spectra for THT in gas phase have also been recorded for different excitation wavelengths between 280 and 234 nm by Myers *et al.* [70]. The results have shown that due to the vibronic effects the overtone and combination bands contribute strongly to the spectra in different excitation frequencies. At least two of those recorded spectra have been dominated by overtone and combination bands. Using the same level of theory as in the calculations of the absorption spectrum, we calculate the resonance and non-resonance Raman spectra for three different excitation frequencies, namely 257, 263 and 286 nm. We include the theoretical and experimental spectra of THT for excitation wavelengths frequencies at (theor. 257 nm, exp. 251 nm), (theor. 263 nm, exp. 257 nm) and (theor. 286 nm, exp. 280 nm) in Fig. (4.2). In addition to the predicted Raman profile for fundamental (0–1), overtone (0-2) and combination frequencies, we have also included the unshifted Raman scattering for the (0–0) transition. The latter clearly dominates the spectra. Under resonance and preresonance conditions, as applied in the calculation of the Raman parameters presented earlier, there is a very close agreement between theory and experiment (Fig. (4.2)). The most noteworthy difference between the resonant and off-resonant spectra is that in the resonant case (257 nm and 263 nm) the intensity of the overtone ($2\nu_5$) and combination modes ($\nu_5 + \nu_{10}$) around 3200 cm^{-1} and 2800 cm^{-1} respectively, is almost as high as that of the fundamental mode ν_{10}, while in the off-resonant case (286 nm), the overtone mode ($2\nu_5$) is depleted from the predicted spectrum, a change which can be seen clearly in the experimental spectra as well (see Fig. (4.2)). The collapse of the first and second overtones is clearly dependent on the shift between the ground and excited state potential surfaces.

The DNA and RNA bases build the most important blocks of life namely the hardware of the genetic code and therefore it is of fundamental importance to understand the photochemical as well as photophysical events and properties in such bases. For instance the absorption spectrum of these bases lie between 200-300 nm [27], which make the living organism vulnerable to sunlight in the

UV range, particularly for the young earth, where it was exposed to massive radiation compared to the situation today [2]. The UV absorbing $^1\pi\pi^*$ excited states of the DNA bases are located about 248 nm (5 eV) above the ground state. However, it has been reported recently that the Watson-Crick structure of the DNA bases exhibit broad UV spectra (short lifetimes of excited states in the order of 10^{-14} s) and there are reactive decay channels (low-lying conical intersections) or dark states that connect the $^1\pi\pi^*$ states with the electronic ground state S_0 [101, 100, 2]. This ultrafast internal conversion mechanism provides photochemical stability by preventing decay of population of the reactive triplet state, but instead it decays back to the ground state. This characteristic property might offer protection to the bases against photochemical damage from UV radiation. As we indicated above, RRS can be used to probe DNA base pairs and thus provide significant structural characterization after the excitation. Experimental resonant Raman spectra of the DNA base pair poly(dG-dC) are available in the work by Foder *et al.* [27] in the wavelengths excitation between 200–266 nm. In Fig. (4.3) we include the theoretical and experimental spectra for DNA at 266 and 265 nm excitation frequency, respectively, in the frequency region 400–2000 cm^{-1}. It is clear from Fig. (4.3) that the positions of the spectral features are almost the same, and just as in the experimental spectrum the scattering intensities are dominated by the peak around 1500 cm^{-1}. With respect to the prediction of intensities for the fingerprint peaks, the agreement between theory and experiment is satisfactory.

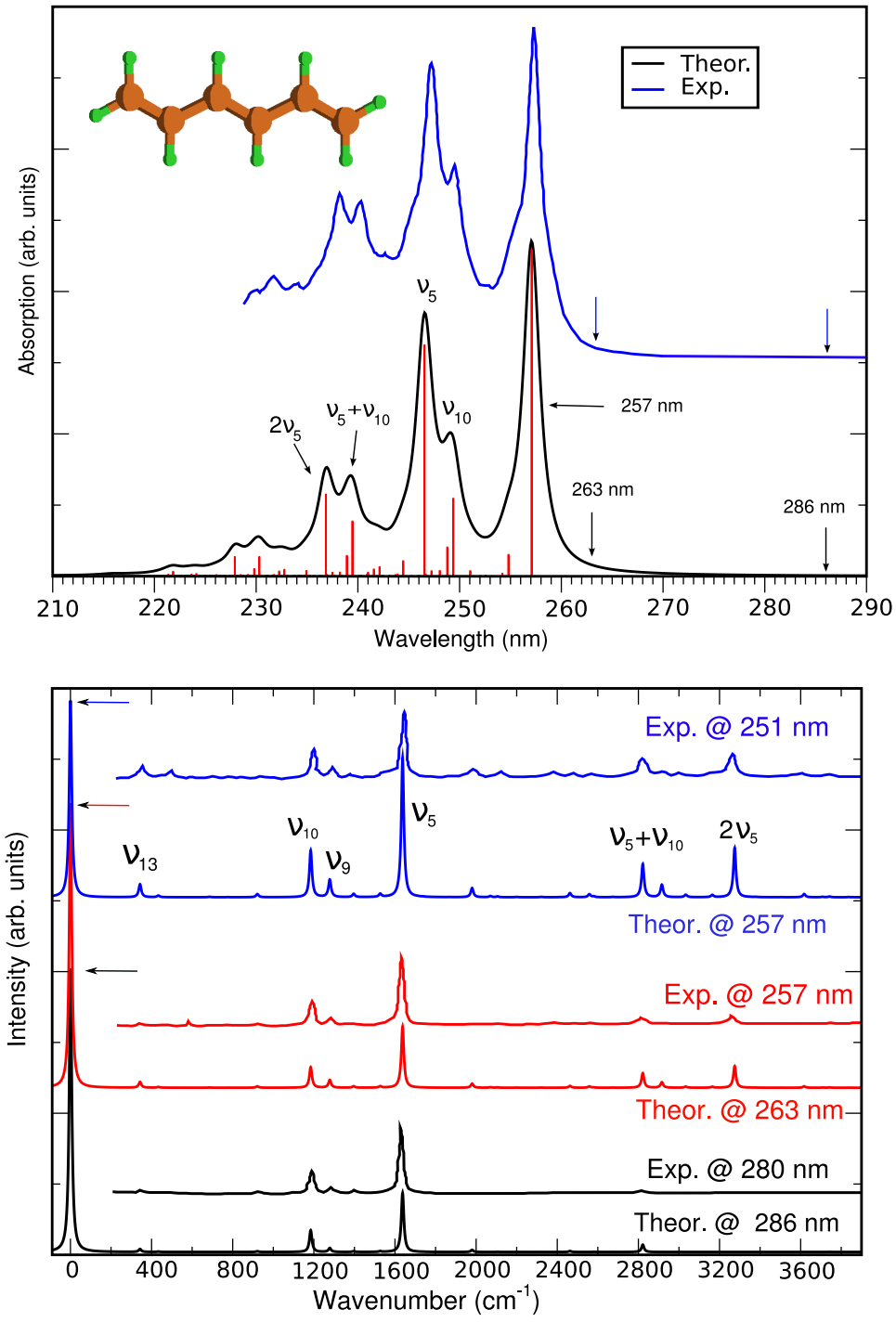

Figure 4.2: UV absorption spectra (upper) and resonant Raman spectra (lower) for THT. The theoretical spectra are broadened by Gaussian line profiles. The experimental spectra are taken from Ref. [70].

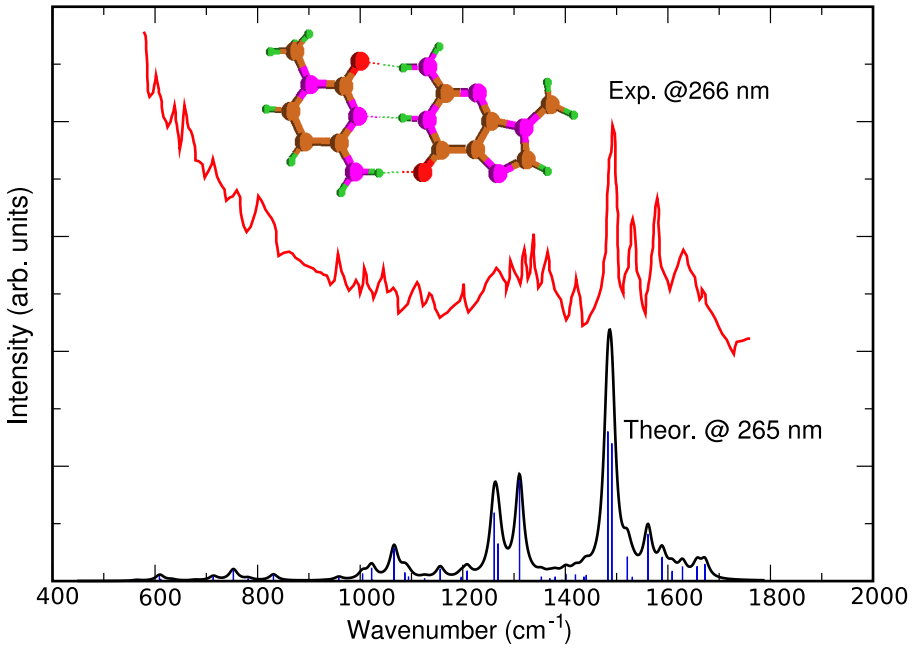

Figure 4.3: Resonant Raman spectrum for DNA is calculated at excitation frequencies 265 nm, using a damping of $\gamma = 0.0045$ a.u. The spectrum has been broadened by a Lorentzian with a width of 20 cm^{-1}. The experimental spectrum is taken from ref. [27].

4.2 Nonlinear Raman scattering

4.2.1 Coherent anti-Stokes Raman scattering (CARS)

As put forward in this thesis resonance Raman scattering (RRS) ranks among the most powerful tools to provide valuable information about structure and function of molecular materials, with the combination of reasonably high resolution and good sensitivity [103, 93, 95, 40]. However, a drawback to the resonance Raman scattering technique is the presence of a fluorescence background, something that can make this technique inapplicable to highly luminescent media as, for instance, biochemical systems [16, 26]. In contrast, coherent anti-Stokes Raman scattering (CARS) has established itself as an important and alternative candidate to probe structure and function of molecules or composite materials in biology, neurobiology, pathology, and pharmacology [26] (see section 2.3.1). In the biomedical area, CARS makes it possible to perform high-resolution imaging of brain tissue which is composed of billions of neurons and support cells to be visualized by tuning the CARS signal into CH_2 vibrational symmetric stretching frequency (2845 cm^{-1}) [26]. Since CARS penetration depth is small, compared to the penetration depth of e.g. NMR signals, CARS offers a possibility to investigate subcellular structures with high spatial and time resolution [96]. CARS can also be applied in nanostructures [48, 113] and nanocomposite materials. Additional advantages of CARS for biological applications is its high energy conversion, its insensitivity towards fluorescence and its excellent time resolution [97]. This short list of advantages and applications have motivated the strong development made in the field for CARS during the past two decades. Moreover, many opportunities for pushing the fundamental limits of CARS microscopy continue to be unraveled [26, 103, 93, 95, 40, 97, 14]. CARS can potentially also be useful in the field of stand-off detection of foreign substances in gaseous form or in interaction with substrates [12, 82]. Operation at ultra-low intensities is most often required in order to detect single molecules or microscopic objects for which the basic Raman cross section generally is very small. For instance the normal Raman process yields only one inelastically scattered photon in 10^6-10^8 incident photons (see section 2.2.2), while in CARS yields one anti-Stokes photon in 10^2-10^3 incident photons which represents a gain for CARS of more than four orders of magnitude. The latter can be demonstrated by comparing the normal Raman intensity of 1,3,5-trinitro-1,3,5-triazacyclohexane (RDX) explosive with the corresponding CARS signal [65]. In Fig. 4.4 we present the calculated non-resonant Raman differential cross sections and CARS spectrum for RDX in gas phase for the frequency region 800–1400 cm^{-1} at a wavelength of 532 nm. The experimental CARS (upper) and Raman (lower) spectrum for RDX was reported and analyzed in the work of Portnov *et al.* [82] and are shown as inset in Fig. 4.4.

The optimized molecular structures of the RDX molecule belong to the point

group C_{3v} which has been found to be the most stable conformer among the six different conformations in gas phase [108]. In our calculation the force fields are determined using the hybrid B3LYP exchange–correlation functional [8, 52, 62, 109] together with the double-ζ basis set (cc-pVDZ). In the calculations of the polarizabilities and second hyperpolarizabilities, we use a Hartree–Fock wave function in combination with the cc-pVDZ basis set. The derivatives of the polarizability tensor with respect to nuclear displacements are determined at the B3LYP equilibrium geometries and with the normal coordinates of the mentioned force fields. The geometry optimization and the calculations of force fields have been performed with the Gaussian program [29], whereas the polarizabilities and second hyperpolarizability calculations have been carried out with the Dalton program [1]. The calculated spectra which are shown in Fig. 4.4 reveal that all the symmetric modes contribute strongly to the spectra of the studied molecule, but quite differently so for the CARS and Raman spectra, since the power of the generated CARS signal is proportional to $P_{CARS} \propto [\alpha_{\alpha\beta}]^4$ while the comparable relation for normal Raman effect is the Raman intensity $I_{RAMAN} \propto [\alpha_{\alpha\beta}]^2$. The forth power dependence in the transition polarizability tensor ($\alpha_{\alpha\beta}$) in CARS leads generally to that the strong lines become stronger than their weaker neighbors.

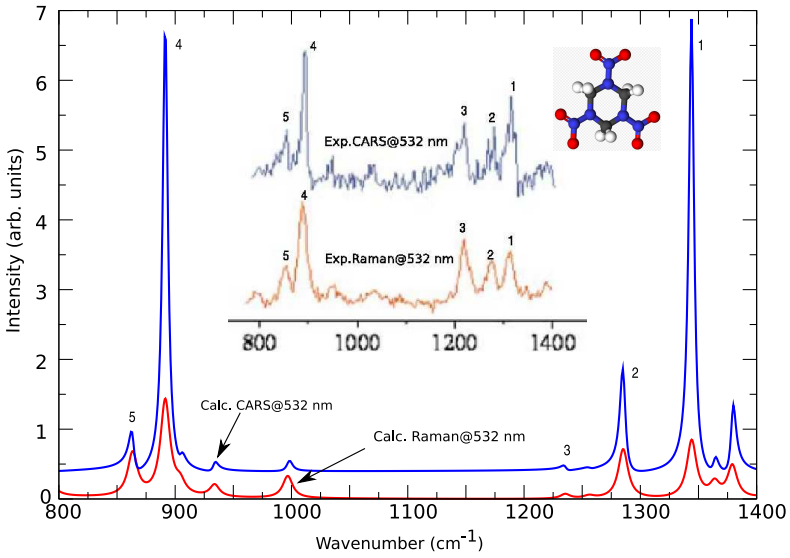

Figure 4.4: Calculated CARS and non-resonant Raman spectra for RDX at 532 nm. The inset shows the experimental CARS and non-resonant Raman spectra, which is taken from Ref. [82].

Bibliography

[1] *DALTON, a molecular electronic structure program, Release 2.0 (2005),see http://www.kjemi.uio.no/software/dalton/dalton.html*, 2005.

[2] A. Abo-Riziq, L. Grace, E. Nir, M. Kabelac, P. Hobza, and M. S. de Vries. *PNAS*, 102:20, 2005.

[3] W. P. Acker, D. H. Leach, and R. K. Chang. *Chem. Phys. Lett.*, 155:4,5, 1989.

[4] A. C. Albrecht. *J. Chem. Phys.*, 34:1476, 1961.

[5] E. M. K. Annika, K. Tae-Woong, O. Jeankun, H. Martin, S. Slobodan, F. S. Michael, and H. L. Gary. *Opt. Lett.*, 27, 2002.

[6] P. W. Atkins. *Molecular Quantum Mechanics*. Oxford University Press, New York, 2001.

[7] A. D. Becke. *Phys. Rev. Lett.*, 38:3098, 1988.

[8] A. D. Becke. *J. Chem. Phys.*, 98:5648, 1993.

[9] D. M. Bishop and Kirtman B. *J. Chem. Phys.*, 95:2646, 1991.

[10] D. M. Bishop and Kirtman B. *J. Chem. Phys.*, 97:5255, 1992.

[11] D. M. Bishop, J. M. Luis, and B. Kirtman. *J. Chem. Phys.*, 108:10013, 1998.

[12] A. Blanco, L. C. Pacheco-Londono, A. J. Pena-Quevedo, and S. P. Hernandez-Rivera. *Proc. SPIE*, 6217:621737, 2006.

[13] R. Boyd. *Nonlinear Optics*. Academic Press Limited, United Kingdom, 1992.

[14] A. L. Carreira and L. M. Horovitz. *Non-Linear Raman Spectroscopy and its Chemical Applications*. D. Reidel Publishing Company, England, 1982.

[15] B. Charles. *The Coherence of the Arabic-Latin Translation Program in Toledo in the Twelfth Century*, page 249. Cambridge: Harvard Univ. Pr., 2001.

[16] J. Cheng, A. Volkmer, and X. Sunney. *J. Opt. Soc. Am.*, 19:1363, 2002.

[17] Z. Chi and S. Asher. *J. Phys. Chem. B*, 102:9595, 1998.

[18] L. Chinsky, A. Laigle, W. L. Peticolas, and P-Y. Turpin. *J. Chem. Phys.*, 76:1, 1981.

[19] R. J. H. Clark and R. E. Hester. *Advances in Non-linear Spectroscopy.* John Wiley and Sons, New York, 1987.

[20] V. Couling, P Fischer, D. Klenerman, and W. Huber. *Biophysical Journal*, 75:1097, 1998.

[21] J. E. Curtis and Reade J. E. Art and empire: treasures from Assyria. British Museum, London, 1995.

[22] J. C. Decius and J. E. Rauch. page 48, 1959.

[23] P. A. M. Dirac. *Proc. R. Soc. London, Ser. A.*, 114:710, 1927.

[24] T. H. Dunning Jr. *J. Chem. Phys.*, 90:1007, 1989.

[25] A. Ehlerding, I. Johansson, S. Wallin, and H. Östmark. *Swedish Defense Research Agency (FOI).*, 2009.

[26] C. L. Evans and S. X. Xie. *Annu. Rev. Anal. Chem.*, 1:883, 2008.

[27] S. P. A. Fodor and T. G. Spiro. *J. Am. Chem. Soc.*, 108:3198, 1986.

[28] P. Frank, A. E. Hill, C. W. Peters, and G. Weinreich. *Phys. Rev. Lett.*, 7:118, 1961.

[29] M. J. Frisch, G. W. Trucks, H. B. Schlegel, G. E. Scuseria, M. A. Robb, J. R. Cheeseman, V. G. Zakrzewski, J. A. Montgomery, R. E. Stratmann, J. C. Burant, and etal. Gaussian 98, Gaussian Inc., Pittsburgh PA, 1998. See http://www.gaussian.com.

[30] F. Gel'mukhanov and H. Ågren. *J. Elect. Spect. Rel. Phen.*, 88:29, 1998.

[31] F. Gel'mukhanov and H. Ågren. *Phys. Rep.*, 312, 1999.

[32] H. Goldstein. *Classical Mechanics.* Addison wesley, San Francisco, 2002.

[33] W. Greiner. *Quantum Mechanics: An introduction.* Springer, New Yourk, 1989.

[34] J. Guthmuller and B. Champagne. *J. Chem. Phys.*, 127:164507, 2007.

[35] E. J. Heller, R. Sundberg, and D. Tannor. *J. Phys. Chem.*, 86:1822, 1982.

[36] B. A. Hess, L. J. Schaad, P. Carsky, and R. Zahradnik. *J. Chem. Rev.*, 86:709, 1986.

[37] H. J. Hibben. *The Raman Effect and Its Chemical Applications*. Reinhold Publishing Company, New York, 1939.

[38] P. Hohenberg and W. Kohn. *Phys. Rev. Lett.*, 136:864, 1964.

[39] J. M. Hollas. *Modern Spectroscopy*. John Wiley & Sons, New Yourk, 1996.

[40] M. Husanu, M. Baibarac, N. Preda, and I. Baltog. *J. Optoelect. Adv. Mat.*, 10:1722, 2008.

[41] Pearsall J. *The New Oxford Dictionary of English*. Oxford University press, England, 2001.

[42] F. Jensen. *Introduction to Computational Chemistry*. John Wiley & Sons Ltd, England, 2003.

[43] L. Jensen, J. Autschbach, and G. C. Schatz. *J. Chem. Phys.*, 122:224115, 2005.

[44] L. Jensen and G. C. Schatz. *J. Phys. Chem. A*, 110:5973, 2006.

[45] L. Jensen, L. Zhao, J. Autschbach, and G. C. Schatz. *J. Chem. Phys.*, 123:174110, 2005.

[46] L. Jensen, L. Zhao, J. Autschbach, and G. C. Schatz. *J. Chem. Phys.*, 123:174110, 2005.

[47] W. Kiefer and D. A. Long. *Non-linear Raman Spectroscopy and its Chemical Applications: General Introduction To Non-linear Raman Spectroscpy*. D. Reidel, England, 1982.

[48] S. O. Konorov, V. P. Mitrokhin, I. V. Smirniova, D. A. Sidorov-Biryukov, A. B. Fedotov, and A. M. Zheltikov. *J. Raman. Spec.*, 36:171, 2005.

[49] H. A. Kramers and W. Heisenberg. *Z. phys.*, 31:681, 1925.

[50] A. Krista and L. Jensen. *J. Phys. Chem. C*, 12(114):5540, 2010.

[51] W.V. La Via, J. L. Lambert, M. J. Pelletier, J. M. Morookian, S. J. Sirk, D. Mickiene, T. J. Walsh, and M. S Borchert. *Med Mycol.*, 44(2):169–74, 2006.

[52] C. T. Lee, W. T. Yang, and R. G. Parr. *Phys. Rev. B*, 37:785, 1988.

[53] Soo-Y Lee. *J. Chem. Phys.*, 2:78, 1983.

[54] Soo-Y Lee and E. J. Heller. *J. Chem. Phys.*, 12:71, 1979.

[55] D. C. Lindberg. *Alhazen's theory of vision and its reception in the west.* The university of Chicago Press, USA, 1967.

[56] D. C. Lindberg. *Theories of vision from al-kindi to kepler.* The university of Chicago Press, USA, 1976.

[57] D. A. Long. *Raman Spectroscopy.* McGraw-Hill, New York, 1977.

[58] D. A. Long. *The Raman Effect.* John Wiley & Sons Ltd., West Sussex, England, 2002.

[59] P. D. Maker and R. W. Terhune. *Phys. Rev. A*, 137:801, 1965.

[60] S. M. McMurry. *Quantum Mechanics.* Addison Wesley, England, 1996.

[61] B. Mennucci, C. Cappelli, R. Cammi, and J. Tomasi. *Theor. Chem. Acc.*, 117:1029, 2007.

[62] B. Miehlich, A. Savin, H. Stoll, and H. Preuss. *Chem. Phys. Lett.*, 157:200, 1989.

[63] A. Mohammed, H. Ågren, and P. Norman. *Chem. Phys. Lett.*, 468:119, 2009.

[64] A. Mohammed, H. Ågren, and P. Norman. *Phys. Chem. Chem. Phys.*, 11:4539, 2009.

[65] A. Mohammed, H. Ågren, A. J. Thorvaldsen, and K. Ruud. *Chem. Phys. Lett.*, 485:325, 2010.

[66] A. Mohammed, B. Minaev, H. Ågren, M. Lindgren, and P. Norman. *Chem. Phys. Lett.*, 481:209, 2009.

[67] H. Mohapatra and S. Umapathy. *Chem. Phys. Lett.*, 390:427, 2004.

[68] S. Mukamel. *Principles of Nonlinear Optical Spectroscopy.* Oxford University press, New York, 1995.

[69] A. B. Myers. *J. Raman. Spec.*, 28:389, 1997.

[70] A. B. Myers and K. S. Pranata. *J. Phys. Chem.*, 93:5079, 1989.

[71] A. K. Myers. *Annu. Rev. phys. Chem.*, 61:41, 2010.

[72] J. Neugebauer. *Phys. Rev.*, 489:1, 2010.

[73] J. Neugebauer and B. A. Hess. *J. Chem. Phys.*, 120:11564, 2004.

[74] W. Nicholas. *Perception*, 28:1115, 2001.

[75] P. Norman. *Nonlinear Optical Properties of Fullerenes, Oligomers, and Solution*. Linköping University, Sweden, 1998.

[76] P. Norman, D. M. Bishop, H. J. Jensen, and J. Oddershede. *J. Chem. Phys.*, 123:194103, 2005.

[77] P. Norman, D. M. Bishop, H. J. Aa. Jensen, and J. Oddershede. *J. Chem. Phys.*, 115:10323, 2001.

[78] P. Norman and K Ruud. *Nonlinear optical properties of matter: from molecules to condensed phases, chapter titled Microscopic theory of nonlinear optics*. Kluwer, Dordrecht, 2006.

[79] J. Olsen and P. Jørgensen. *J. Chem. Phys.*, 82:3235, 1985.

[80] B. J. Orr and J. F. Ward. *Mol. Phys.*, 20:513, 1971.

[81] T. Petrenko and F. Neese. *J. Chem. Phys.*, 127:164319, 2007.

[82] A. Portnov, S. Rosenwaks, and I. Bar. *App. Phys. Lett.*, 93:041115, 2008.

[83] T. Privalov. *Electronic and nuclear dynamics of X-ray processes*. Universitetsservice US AB, Stockholm, 2001.

[84] T. Privalov, F. Gel'mukhanov, and H. Ågren. *Phys. Rev. B*, 59:14, 1999.

[85] M. Puranik, J. Chandrasekhar, J. G. Snijders, and S. Umapathy. *J. Phys. Chem. A*, 105:10562, 2001.

[86] O. Quinet and B. Champagne. *J. Chem. Phys.*, 117:2481, 2002.

[87] O. Quinet and B. Champagne. *J. Chem. Phys.*, 124:244312, 2006.

[88] O. Quinet, B. Champagne, and V. Rodriguez. *J. Chem. Phys.*, 121:4705, 2004.

[89] R. Rashed. *Encyclopedia of the History of Arabic Science*. Routledge, United Kingdom, 1996.

[90] P. R. Regnier and J. P. E. Taran. *App. Phys. Lett.*, 23:240, 1973.

[91] V. Rodriguez, D. Talaga, F. Adamietz, J. L. Bruneel, and M. Couzi. *App. Phys. Lett.*, 431:190, 2006.

[92] T. Rush III and W. L. Peticolas. *J. Phys. Chem.*, 99(40):14647, 1995.

[93] M. Rybachuk, A. Hu, and J. M. Bell. *App. Phys. Lett.*, 93:051904, 2008.

[94] P. Salek, O. Vahtras, T. Helgaker, and H. Ågren. *Phys. Chem. Chem. Phys.*, 5:1, 2003.

[95] S. Sangdeok, C. M. Stuart, and R. A. Mathies. *Chem. Phys. Chem.*, 9:697, 2008.

[96] R. D. Schaller, J. Ziegelbauer, L. F. Lee, L. H. Haber, and R. J. Saykally. *J. Phys. Chem. B*, 106:8489, 2002.

[97] W. F. Schneider. *Non-Linear Raman Spectroscopy and its Chemical Applications*. D. Reidel Publishing Company, Netherlands, 1982.

[98] C V. Sheth. *J. Phys. B: Atom. Molec. Phys.*, 8:1, 1975.

[99] T. I. Sideroudi, N. M. Pharmakakis, G. N. Papatheodorou, and G. A. Voyiatzis. *Lasers in Surgery and Medicine.*, 38:695, 2006.

[100] A. L. Sobolewski and W. Domcke. *Phys. Chem. Chem. Phys.*, 6:2763, 2004.

[101] A. L. Sobolewski, W. Domcke, and C. Hättig. *PNAS*, 102:17903, 2005.

[102] A. Szabo and S. N. Ostlund. *Modern Quantum Chemistry*. McGraw–Hill, New York, 1989.

[103] Z. K. Tang, J. P. Zhai, Y. Y. Tong, X. J. Hu, R. Saito, Y. J. Feng, and Ping Sheng. *Phys. Rev. Lett.*, 101:047402, 2008.

[104] R. W. Terhune, P. P. Maker, and C. M. Savage. *Phys. Rev. Lett.*, 14:681, 1965.

[105] A. J. Thorvaldsen, L. Ferrighi, K. Ruud, H. Ågren, P. Jørgensen, and S. Coriani. *Phys. Chem. Chem. Phys.*, 11:2293, 2009.

[106] A. J. Thorvaldsen, K. Ruud, K. Kristensen, P. Jørgensen, and S. Coriani. *J. Chem. Phys.*, 129:214108, 2008.

[107] M. W. Tolles, W. J. Nibler, R. J. Mcdonald, and B. A. Harvey. *J. App. Spec.*, 31:4, 1977.

[108] T. Vladimirroff and M. B. Rice. *J. Phys. Chem. A*, 106:10437, 2002.

[109] S. H. Vosko, L. Wilk, and M. Nusair. *Can. J. Phys.*, 58:1200, 1980.

[110] S. O. Williams and D. G. Imre. *J. Phys. Chem.*, 92:3363, 1988.

[111] T. Yanai, D. P. Tew, and N. C. Handy. *Chem. Phys. Lett.*, 393:51, 2004.

[112] W. Yang and G. C. Schatz. *J. Chem. Phys.*, 97:5, 1992.

[113] A. M. Zheltikov. *Laser Phys. Lett. 1*, 9:468, 2004.